Quaternary Science Reviews
January 2021, Volume 252 Pages 106722 (15p.)
https://doi.org/10.1016/j.quascirev.2020.106722
https://archimer.ifremer.fr/doc/00664/77652/

Ocean surface and bottom water conditions, iceberg drift and sediment transport on the North Iceland margin during MIS 3 and MIS 2

Andrews J.T. [1,*], Smik L. [2], Belt S.T. [2], Sicre M.-A. [3], McCave I.N. [4]

[1] Institute of Arctic and Alpine Research, Department of Geological Sciences, University of Colorado, Boulder, CO, 80303, USA
[2] Biogeochemistry Research Centre, School of Geography, Earth and Environmental Sciences, University of Plymouth, Drake Circus, Plymouth, PL4 8AA, UK
[3] LOCEAN, CNRS, Sorbonne Université, Campus Pierre et Marie Curie, 4 Place Jussieu, Paris, France
[4] Godwin Laboratory for Palaeoclimate Research, Department of Earth Sciences, University of Cambridge, Downing Street, Cambridge, CB2 3EQ, UK

* Corresponding author : J. T. Andrews, email address : andrewsj@colorado.edu

Abstract :

Radiocarbon dates and marine tephra suggest that the upper 10 m of core MD99-2274 off North Iceland extends from ~0 to ~65 ka BP. A multi-proxy sediment and biomarker study at a ~0.5 ky resolution is used to derive a paleoclimate scenario for this area of the southwestern Nordic Seas, which during the Holocene had intermittent excursions of icebergs and a seasonal cover of drifting sea ice across the site. The sortable silt mean size ($\overline{SS}$) suggests a bottom current (1000 m depth) flow speed maximum to minimum range of ~8 cm/s during Marine Isotope Stages 2–3, but the data are unreliable for the Holocene. Slow-down in flow speeds may be associated with massive ice and water discharges linked to the Hudson Strait ice stream (H-events) and to melt of icebergs from Greenland in the Nordic seas where convection would have been suppressed. Five pulses of sediment with a distinct felsic component are associated with iceberg transport from E/NE Greenland. Sea ice, open water and sea surface temperature (SST) biomarker proxies (i.e. IP25, HBI III, brassicasterol and alkenones) all point towards near-perennial sea ice cover during MIS 3 and 2, rather than seasonal sea ice or open water conditions. Indeed, our biomarker and sediment data require that the seas north of Iceland experienced a nearly continuous cover of sea ice, together with icebergs calved from ice stream termini, which drifted southward. The cross-correlation of the quartz % records between MD99-2274 and the well-dated core PS2644 in Blosseville Basin indicates significant coherence in the records at a multi-millennial (~8 ky) timescale. A transition to open ocean conditions is evident from the early Holocene onwards, albeit with the occurrence of some drift ice and icebergs.

Highlights

► Multi-proxy biogeochemical, grain-size, and mineral analysis. ► MIS 2 and 3 record of sea ice cover and ice-rafting in the Iceland Sea. ► HBI, sterol and alkenone biomarkers point to extensive sea ice during MIS 3 and MIS 2. ► Episodes of quartz input linked to a NE source (s) ► Bottom currents at 1000 m depth combine THC Nordic outflow and saline density flow.

Keywords : Iceland Plateau, MIS 2 and 3, Sea ice biomarkers, IP25, Alkenones, Sortable silt, Sediment provenance

1. Introduction

1.1 Aims of study

In order to gain some understanding of the complex marine environments that prevailed during the Late Quaternary we need to employ a multi-proxy approach that not only characterizes ocean surface and bottom water conditions, but also provides direct measurement of glacial influences on sediment supply. Several studies have been reported from the North Iceland Shelf (Fig. 1) that document late glacial/Holocene records (e.g. Andrews et al., 2018; McCave and Andrews, 2019a & b; Sicre et al., 2008; Knudsen et al., 2003) but there are only limited references to conditions during Marine Isotope Stages (MIS) 2, 3 or 4. Therefore, with the primary goal of establishing a framework for environmental conditions in this sector of the Iceland Sea from MIS 2 to MIS 4, we selected a previously unstudied core, MD99-2274 (Labeyrie et al., 2003) (Fig. 1), and sampled the upper 10 m. MD99-2274 (henceforth #2274) is a 10-cm diameter 26 m Calypso core retrieved from 67.582°N and 17.073°W at 1000 m water depth (Labeyrie et al., 2003) during the IMAGES V cruise aboard the French RV *Marion Dufresne*. For further context, we note that the core site is located 200 km east of the well-studied core PS2644 (van Kreveld et al., 2000; Voelker, 1999; Voelker and Haflidason, 2015) and 163 km from core P57-7 (Sejrup et al., 1989) (Table 1, Fig. 1A). The main questions we posed were: 1) what is an appropriate depth/age model, 2) is there evidence for either pervasive sea ice or an ice shelf (Boers et al., 2018; Dokken et al., 2013; Petersen et al., 2013), which have been called for to explain D-O cycles, 3) what were sea surface temperatures (SSTs), and 4) are there substantial changes in grain-size and mineral composition that can be associated with changes in bottom current flow speed and changes in glacial sediment provenance? Given the location of the core (Fig. 1A) we were particularly interested in whether we could discriminate between glacial sediments derived from Iceland versus those from E/NE Greenland.

1.2 Present-day oceanography

The Iceland and Greenland Seas (Fig. 1A) are key areas for the formation of dense overflow waters (Brakstad et al., 2019) that flow south through sills in the Scotland-Greenland Ridge (Fig. 1C). The North Icelandic Jet (NIJ) flows southwestward along the slope below ~1000 m (Fig. 1C) with a mean speed of 9.3 m ± 2.7m/sec towards Denmark Strait (Mauritzen, 1996; Pickart et al., 2005) where it exits to form a major component of North Atlantic Deep Water *"….and points to the Iceland Sea as an important place for this water mass formation."* (Jonsson and Valdimarsson, 2004). The study site lies in a sensitive area with the surface flow being the East Icelandic Current (EIC), which brings cold and relatively fresh surface water as a spin-off from the East Greenland Current (EGC), whereas the North Icelandic Irminger Current (NIIC), sourced from the southern warmer and saltier waters of the North Atlantic Drift (Stefansson, 1962), continues as an eastward flow over the inner North Iceland Shelf (NIC) (Fig. 1C).

Sea ice in the form of drift ice has been noted to reach the area in modern times, although the average position of the sea ice edge (30% sea ice cover by area) lies north of our site (Divine and Dick, 2006) (Fig. 1C). Thirty years of observations on the presence of icebergs (Andrews et al., 2019), their Fig. 7A) indicate that icebergs from E/NE Greenland drift across the site.

1.3 Background to study region

Stein and colleagues (Nam et al., 1995; Stein, 2008; Stein et al., 1996) studied a comprehensive suite of cores on the Scoresby Sund Trough Mouth Fan (Fig. 1A, TMF) and reported both ice-rafted debris (IRD) and $\delta^{18}O$ on the near-surface planktonic foraminifera *Neoglobquadrina pachyderma* (Table 1). The cores included discrete IRD peaks (counts 10 cm^3 > 500 µm), which they suggested may have been coeval with the massive ice and water discharges of the Hudson Strait Heinrich (HS H-) events (Andrews and Voelker, 2018b; Heinrich, 1988; Hemming, 2004; Hesse 2016). However, whether the response of the Greenland, Iceland, and European ice sheets was synchronous or asynchronous with the Laurentide Ice Sheet collapse events still requires clarification (Dowdeswell et al., 1999; Elliot et al., 2001). Verplanck et al (2009) provided radiogenic isotope data fingerprinting sediment sources from two cores on the Scoresby Sund TMF (O'Cofaigh et al., 2002) (JR51-GC31 and -GC32) and another core (PS62/017-4) from the Blosseville Basin (Milo et al., 2005) (Table 1). Stein et al. (1996) and Verplanck et al. (2009) described events in cores PS1730 and PS62/017-4 (Table 1, Fig. 1) that they considered coeval with the HS H-events. Andrews and Voelker (2018) have argued that the use of the term "Heinrich events" for locations such as the Nordic Seas is not appropriate and should be modified. For example, the IRD-rich layer in PS2644 correlated with HS H-2 (Voelker et al., 1998) is now referred to as PS2644 IRD#2 (Andrews and Voelker, 2018). In our study, events that might correlate with HS H-events will be termed #2274-IRD#.

There is no firm agreement on the extent and duration of sea ice cover in the Nordic Seas during MIS 2 and MIS 3. The CLIMAP data showed an extensive cover across the Nordic Seas (Ruddiman and McIntyre, 1981) whereas Sarnthein et al. (2003)

argue that the Nordic Seas during MIS 2 were "..largely ice free" during the summer months. The presence of an ice shelf buttressing the East Greenland ice streams has also triggered a debate especially as to a possible answer to the cause of D-O oscillations (Pettersen et al., 2013; van Kreveld et al., 2000). However, other researchers working at sites in the eastern Nordic Seas have rather focused on the role of sea ice (Dokken et al., 2013; Hoff et al., 2016) and changes in the structure of the water column, and concluded that during Greenland interstadials in MIS 3, sea ice was limited in extent and duration.

The presence of thick, pervasive sea ice could potentially limit the export of icebergs from E and NE Greenland Ice Streams (Reeh et al., 1999), although the sediment records from numerous sediment cores retrieved from the floor of the Arctic Ocean clearly document that iceberg rafting occurred throughout the Pleistocene (Clark, 1990a,b; Stein, 2008; Phillips and Grantz, 2001; Stokes et al., 2005), with some evidence that the timing of events in some cores were similar to those for HS H-events. For example, IRD peaks in cores from the Arctic Ocean were linked to the McClure Ice Stream in the NW sector of the Laurentide Ice Sheet and dated at 12.9, 15.6, ~22, and 30 ka BP (Stokes et al., 2005). Iceberg drift is primarily a function of the integrated current direction and speed over depth, plus a component associated with wind forcing on the exposed "sail" (Bigg, 2016). In many ways, sea ice protects icebergs as it inhibits wave action, which is the greatest cause of iceberg disintegration (Bigg, 2016; Venkatesh et al., 1994).

1.4 Ice sheet extent MIS 1 to MIS 3

#2274 lies only 60 km north of the LGM limit of the Iceland Ice Sheet (IIS) (Fig. 1) (Andrews and Helgadottir, 2003; Patton et al., 2017) with the onset of retreat associated with calibrated radiocarbon dates of between 14 and 15 ka BP, depending on the ocean reservoir correction (Andrews et al., 2018; Andrews and Helgadottir, 2003; Knudsen et al., 2003). Retreat from the maximum position was rapid (Andrews et al., 2018; Norðdahl and Ingolfsson, 2015; Patton et al., 2017), and the ice sheet was at or behind the present-day coast by the time of the deposition of the Vedde tephra ~12.2 ka BP (Lohne et al., 2013). Little detail is known about the history of this ice sheet during MIS 3 (e.g. Andrews et al., 2017). Moles et al. (2019) argued that the North Atlantic Ash Zone II (NAAZII) tephra, dated ca 54 ka BP (Austin and Hibbert, 2012), was erupted under >400 m of ice, thus indicating a reasonably extensive IIS during the Greenland ^{18}O stadial 15.2 (Moles et al., 2019; Rasmussen et al., 2014), but no specific information is currently available on the MIS 3 history of the ice sheet.

The Greenland Ice Sheet (GIS) extended to the shelf break during the LGM (Funder et al., 2011b; Vasskog et al., 2015) but little is known about its history during MIS 3 or MIS 4. Judging from the delivery of quartz-rich sediments to cores along Denmark Strait, especially PS2644 and MD99-2323 (Andrews and Vogt, 2020a), it is probable that the ice also reached a similar position at these times. Peterson et al. (2013) suggested that an ice shelf may have extended out from the East Greenland Shelf across Blosseville Basin, although the sedimentary evidence for this is scanty (Andrews and Vogt, 2020a).

1.5 Bedrock Geology and source signatures

In terms of the mineral composition of #2274 sediments, the bedrock in glacial source areas consists primarily of either mafic (basalt) or felsic (granites/gneisses/sandstones), although finer source identification is possible (Andrews and Vogt, 2014; 2020) (Fig. 1A). Further, Andrews and Vogt (2014) demonstrated that the sediment mineral signature of sediments offshore from the Caledonian Fold Belt was dominated by high wt% of quartz, illite, and muscovite. Detrital carbonate sediments derived from the Paleozoic outcrops of N Greenland and the Canadian Arctic are also recognized by color and mineralogy. However, radiogenic isotopes (White et al., 2016; Verplanck et al., 2009) allow more age-related differentiations, which in terms of our region (Fig. 1A and B), consists of Archaean, Paleoproterozoic, Caledonian Fold Belt, and Tertiary volcanics (Henriksen, 2008).

2. Environmental proxies and age model

2.1 Data methods

The proxies used in this paper are the sea ice biomarkers IP_{25} and HBI II (Belt et al., 2007; Belt and Müller, 2013; Belt, 2018), brassicasterol and HBI III as indicators of open water primary production (Volkman, 1986; Belt et al., 2015), alkenones (for SST) (Sicre et al., 2008a), % C37:4 alkenone to identify polar surface waters, grain-size indicators of bottom flow and deposition (McCave and Andrews, 2019a, b; McCave et al., 2017), magnetic susceptibility, and quantitative X-ray diffraction estimates of mineral wt% (Andrews et al., 2017; Andrews and Vogt, 2014). The X-ray diffraction data for #2274 are available (Andrews and Vogt, 2020b) The full details of these methods are included as Supplementary Material.

2.2 Depth/age model

The age model is based on radiocarbon dates and the occurrence of tephras (Table 2). There are significant problems associated with obtaining and interpreting calibrated ages because of the uncertainty of the ocean reservoir correction (ORC), which has varied spatially and temporally, and might be as much as 1000 yr (Andrews et al., 2018; Skinner et al., 2019; Voelker, 1999; Voelker et al., 1998). Three radiocarbon dates were obtained on the near-surface planktonic foraminifera *Neogloboquadrina pachyderma* and the other on lustrous shell fragments. Most tephras older than the Borrobol (ca 14.5 ka BP) (Lind et al., 2016; Matthews et al., 2011) are dated by reference to GIS cores, which themselves are based on a variety of assumptions and whose error increases with the estimated age (Boers et al., 2017). The qXRD data (Andrews et al., 2013; 2018) suggest the presence of high wt% of volcanic glass in two cores on the Iceland Shelf that might be coeval with the Vedde and NAAZII tephras (Brendryen et al., 2011; Lohne et al., 2013). The tephra bed at 607 cm in #2274 was identified by Haflidasson (person. commun. 2018) as being similar to FMAZ IV dated at ~47.12 ka BP (Davies et al., 2008; Rasmussen et al., 2003; Voelker and Haflidason, 2015) and that date is used in our depth/age models (see Supplementary Material). Other discrete layers of black basaltic glass were noted in the shipboard log at 99, 127.5, 717, and 740 cm (Labeyrie et al., 2003, p 477), and age estimates were obtained from our depth/age model (see later).

We used the Bayesian radiocarbon calibration program "Bacon" (Blaauw and Christen, 2005) to construct depth/age models, but we also acknowledge the many problems associated with establishing accurate depth/age models (Telford et al., 2003; Trachsel and Telford, 2017). The first model is based solely on the available ^{14}C dates and the 607 cm tephra (Table 2A and B), while the second one is based on an assumed age estimate for the core top of 500 ± 500 (i.e. little sediment loss) and the inferred presence of the Vedde and NAAZII tephras. Given the uncertainty in the OCR, we used a ΔR = 0. In practice, there is relatively little difference in the median age estimates (Fig. 2A). The average sediment accumulation rate (SAR) is 68 yr/cm or 14.7 cm/ky, thus our 10 cm sampling density permits millennial-scale evaluations, with an average spacing between samples of 0.5 cal ky. Remarkably, for MD cores of this vintage (1999), the upper part of the core shows no evidence of piston-induced stretching (Skinner and McCave, 2003). However, the spread between minimum and maximum age estimates is often considerable given the relative paucity of dated levels, and the Bayesian approach results in an age estimate for the core top of 3600 yr BP, although the estimated date of 500 ± 500 yr BP finds some support in our data. The estimated ages for the logged tephra layers are: ~11, 13.2, 53, and 56 ka BP. A possible age for the 99 cm basaltic tephra is the 10.2 ka BP Saksunarvatn tephra (Lohne et al., 2013), which is widespread on the north Iceland Shelf (Krisjansdottir et al., 2007; Eiriksson and Knudson, 2002). All our subsequent data have been converted to a common depth/age model using the data in Table 2B; thus, robust inter-proxy comparisons can be made. To ensure that we have not forced our data into an existing framework we have not tuned our model to other records (Blaauw, 2012).

We have also obtained radiocarbon dates on several *Vema* cores that were taken to the north of Iceland and #2274 (Fig. 1; Table 3) (Manley and Jennings, 1996). The calibrated radiocarbon dates range from ~13 to > 49 ka BP (ΔR = 0) and were obtained on relatively large samples of *N. pachyderma* (Table 3). Several tephras were noted in the core description (Suppl. Data), thus indicating that conditions allowed for the deposition of discrete tephras. The dates from these cores also provide additional information on the presence of significant numbers of the planktonic foraminifera *N. pachyderma* (Greco et al., 2019) and hence inferences about sea ice cover and light conditions.

3. Results

3.1 Lithology and Grain-size

The core log of core #2274 (Labeyrie et al., 2003. p. 477) described the sediment as being principally mottled silty clay with colors ranging between 2.5Y4/2 to 5Y4/1. Visible ice-rafted clasts occur but are not common. The grain-size measurements were undertaken on sample splits from the qXRD samples and only 30 samples were processed, resulting in a coarse resolution data set (on average one sample every 2300 yr). The sediments vary between a very coarse to a fine silt with average grain-sizes varying between 54.3 to 6.05 µm. Sand > 240 µm is considered to be ice-rafted (McCave and Andrews, 2019a) and occurs in low % throughout the core, except for two notably coarser intervals with IRD240 > 5%, (Fig. 3).

We have also undertaken an analysis of the sortable silt mean size ($\overline{SS}$) and SS% in the 63-10 µm fractions (McCave et al., 1995). The correlation coefficient between these two variables is r = 0.804 indicating, relative to other cores (McCave and Andrews, 2019a,b), a somewhat noisy correlation, but a generally current-sorted signal (Supplementary Fig. 1). Computation of the running correlation between SS% and $\overline{SS}$ yields high average values (r >0.9) between ~11 and 42 ka BP but values unacceptable for flow speed inference occur in the Holocene and during brief interval ~57 ka BP (Fig. 3). Variations in the flow speed of bottom currents (Fig. 1C) in this region reflect changes in the vigour of the ocean overturning system because the NIJ feeds into the

Denmark Strait overflow, a key starting point for the North Atlantic western Boundary Undercurrent.

The overall range (minimum-maximum) in flow speed indicated by this record is ~8 cm/s. Calibration of the sortable silt proxy yields a sensitivity (cm s^{-1}/µm) rather than an absolute speed-size relationship (McCave et al., 2017). In favourable circumstances actual speeds may be estimated by matching core-top $\overline{SS}$ data to nearby current meter measurements and plotting the differences downcore. Unfortunately, because the Holocene data are unreliable as a speed record, we cannot relate this to the present nearby flow speed measurements of 9.3 cm/sec (Jonsson, 2004). Nevertheless, low speeds correspond to HS H 1 (~15 ka), 4 (~40 ka), and 6 (~60 ka) (Fig. 3) as expected from previous work on the impact of Heinrich and other cold events on N. Atlantic circulation (e.g. Kleiven et al., 2011), on the basis of which, speeds of <5 cm/s are probable.

3.2 Mineral composition

On Figure 4, we plot the changes in the weight % of key minerals as determined by qXRD as well as the ratio quartz/pyroxene, which we use as a measure of felsic/mafic bedrock (as opposed to quartz/plagioclase which was used by Moros et al. (2004)). The quartz wt% in a surface grab from this site is ~5% (Andrews and Eberl, 2007), and the median for the whole record is 5.3 % with a maximum of 16.8 %. The magnetic susceptibility record for #2274 (Fig. 2A) is clearly inversely associated with the variations in quartz (Fig. 2B), which, together with the K-feldspars, are diamagnetic minerals (Robinson et al., 1995; Watkins and Maher, 2003). A similar inverse relationship was noted in other cores from the area (Andrews and Vogt, 2020a). Hence the magnetic susceptibility fluctuations support our interpretation that there are substantial variations in the inputs of felsic- versus mafic-rich sediments.

The Holocene record mimics that from many sites on the North Icelandic Shelf (NIS) in showing an increase in quartz toward the present-day (Andrews et al., 2019). Quartz and pyroxene have an antiphase relationship ($r^2 = 0.47$), which in part is related to the mineral data summing to 100% (i.e. a closed array), and which provides some constraints on the interpretation (Aitchison, 1986; Chayes, 1971). There are five sustained peaks in the quartz wt % (Fig. 4), and K-feldspar (not shown, K-feldspar values track those of quartz (Andrews and Vogt, 2020a)) are therefore not included in this figure), which we interpret as indicating the influx of sediment from NE Greenland and possibly farther afield from Canada or Fennoscandia. Of these possible mechanisms, icebergs alone carry basal and englacial debris that includes all size fractions from cobbles to clay (> 1 μm). The variations in quartz are frequently matched by the sum of calcite and dolomite (carbonate) (Fig. 4) ($r^2 = 0.13$, $p < 0.0001$) although the correlations are much more significant for dolomite ($r^2 = 0.22$) than calcite ($r^2 = 0.07$). This probably represents transport of glacially derived material from the carbonate bedrock of NE and N Greenland and/or the Canadian Arctic Islands and Channels (Darby and Zimmerman, 2008; Lakeman et al., 2018; Phillips and Grantz, 2001). The estimated ages for the 5 peaks are 14.4, 31.5, 40, 54.7, and 61.8 ka BP (Fig. 4) with a possible smaller episode ~22.8 ka BP. These age estimates are somewhat similar to the HS H-events (Andrews and Voelker, 2018a; Heinrich, 1988; Hemming, 2004) (see Fig. 3) but their duration are longer than the <1 ky episodes of detrital carbonate deposition associated with the HS H-events (Andrews and Voelker, 2018a).

Previous work on sediment sources in this area (Verplanck et al., 2009) provide temporally limited but critical information using radiogenic isotopes on the < or > 63µm fractions. Debris flow from the two Scoresby Sund TMF sites (JR51-GC31,-32, Table 1, Fig. 1B) lay along the 1.7 Ga Paleoproterozoic isochron; the samples contained abundant quartz and lesser amounts of basalt (Verplanck et al., 2009, p.53). However, the sediments in the Blosseville Basin (core 17-4, Fig. 1A, Table 1), some 150 km downstream (Fig. 1A), and considered to be coeval with HS H events-1, -2, and -3, all cluster along the 0.5 Ga isochron (Calendonide bedrock, that outcrops on the eastern edge of NE Greenland north of Scoresby Sund (Fig. 1B)). The same isotopic signature characterized the non-HS H sediments in this core. Pb systematics indicate that the Holocene sediment samples at sites 907 (Table 1) and JR51-GC28 are dominated by the 0.5 Ga Calendonides (White et al., 2016). Given the sediment SedUnMix results (Fig. 5) and the reported radiogenic isotopic data (Verplanck et. al., 2009; White et al., 2016), the variations in quartz are most probably associated with sediment discharge events from glacial erosion and transport in ice streams flowing through the numerous fiords north of Scoresby Sund and primarily within the Caledonian Fold Belt outcrop (Evans et al., 2002, 2009; Stein, 2008).

The SedUnMix analysis included sediments from NE Greenland (Calendoides, ~73N; Andrews et al., 2016), E Greenland (basalt), and Iceland. The analysis of possible bedrock sources for the #2274 compositional changes indicated (as might be expected given the bedrock geology of E and NE Greenland, and Iceland) that the NE Greenland source had a granite and gneissic composition, whereas E Greenland and Iceland were linked to basalt and also dolerite (Brooks and Nielsen, 1982; Henriksen, 2008; Higgins et al., 2008; Kristjansson et al., 1979). The results (Fig. 5) indicate that felsic-rich sediments from NE Greenland or farther afield (Arctic Canada, Fennoscandia) (Verplanck et al., 2009) were deposited in a series of events that mimic the influx of quartz to the site (Figs. 2B and 4); the correlation between the NE Greenland Calendonides source estimates in #2274 and the quartz wt% explains 79% of the variance. The average “unaccounted” or “unexplained” composition averaged 20 ± 5 % and degree of fit or average absolute bias is 2.3 ± 0.4 wt% indicating that the input mineral source regions provide a good fit to the #2274 mineral compositions. Figure 5 highlights two periods when the mineral composition indicates little deposition of sediment that could be ascribed to a felsic source centered around 20 and 57 ka BP, the latter being a time of substantial deposition of tephra at this site and also a time when glacial ice covered at least some of Iceland (Moles et al., 2019). Source estimates from E. Greenland (sites seaward of the early Tertiary basalt outcrop on the Geikie Plateau) and SW Iceland resulted in nearly identical patterns over the last ~65 ka BP (Fig. 5), but the results from considering Icelandic basal glacial marine diamictons (Dmm) as a source are different. The reasons for these two differing estimates are presently unclear.

The provenance time-series thus suggests that we can identify four episodes in the arrival of foreign sourced sediments; 1) from ~65 to 38 ka BP when distinct pulses of NE Greenland sourced sediments arrived; 2) 38 to 17 ka BP when there was an overall decrease in this source with virtually no quartz noted ~20 ka BP; 3) a large pulse of these sediments centered ~ 15 ka BP; and 4) the last 10 ka or so that shows a steady increase in this source. This latter event is also noted in MD99-2269 (Fig. 7) and is matched by changes in the sea ice biomarker IP_{25} (Cabedo-Sanz et al., 2016).

3.3 Biomarkers

The sea ice biomarkers IP_{25} and HBI II were absent or below the limit of detection in the majority of the sediment sections analyzed with only a few exceptions (Fig. 6). Of the two, HBI II was always more abundant, consistent with findings from previous studies from the study region and elsewhere in the Arctic (e.g. Massé et al., 2011; Xiao et al., 2013; Bai et al., 2019). In some cases, only HBI II could be identified and quantified, with IP_{25} likely also present in such horizons but below the detection limit.

Alkenones and brassicasterol were found at very low concentrations in glacial sediments contrasting with higher abundances in Holocene sediments. Further, the open water biomarker HBI III was only detected in Holocene sediments (data not shown). While alkenone-SSTs ranged from 7 to 9°C during the Holocene, they are unexpectedly high in the glacial portion of the record, spanning from 8 to 16°C.

4. Discussion

4.1 Icebergs and IRD during MIS 3 and MIS 2

There is no general theory about the association of sea ice and icebergs and there is no observational census of the icebergs being transported in the EGC as there is for the Labrador Shelf off Newfoundland, apart from a 30-yr count of icebergs on the Iceland shelves (Jónsdóttir *in* Andrews et al., 2019). However, Cabedo-Sanz et al. (2016) and Darby et al. (2017) showed that Holocene variations in the wt% of quartz and the sea ice biomarker IP_{25} co-varied in cores to the west and south of #2274, yet this was not the case at #2274 during MIS 2 and MIS 3 (Figs. 4 and 6). In N Greenland, semi-permanent sea-ice conditions prevail today and did so intermittently during the Holocene (Funder et al., 2011a) and it is reasonable to assume that sea-ice would have been more extensive during MIS 2 and MIS 3 when the GIS may have reached the shelf break. However, cosmogenic dates pertaining to the extent of the Northeast Greenland Ice Stream at ~78°N (Larsen et al., 2018) have been used to argue that this ice stream was behind its present margin "…41-26 ka."

Several authors have argued for the presence of an ice shelf fringing the E/NE GIS (Boers et al., 2018; Petersen et al., 2013). However, sediments recovered from beneath ice shelves are invariably fine-grained and lack ice-rafted debris (Domack et al., 1999; Jennings et al., 2019; McKay et al., 2016), whereas the sediments from the Scoresby Sund TMF (Fig. 1) and margin contain clear IRD (Stein et al., 1996) (Fig. 5; see also Table 3). Radiocarbon dates in Stein et al., (1996a) were based on 2000 *N. pachyderma* specimens per sample, and the numerous MIS 2 and MIS 3 radiocarbon dates on *N. pachyderma* from PS2644 (Sarnthein et al., 2003; Voelker, 1999; Voelker et al., 1998, 2000) were obtained on 10 mg samples of 800-2300 tests in 1-cm sediment samples. Although the complete ecology of *N. pachyderma* is not well known, a study of plankton hauls (Greco et al., 2019) indicates a relationship between sea ice cover and chlorophyll, hence suggesting that *"light or light-dependent processes might influence the ecology of this species*." In addition, several of these cores have discrete tephra layers indicating rapid accumulation of tephras by particles falling through the water column, versus a more dispersed occurrence if the tephra was deposited on multi-year sea ice. Together these data indicate that the sea ice, at times during MIS2 and 3 and probably seasonally, must have had extensive leads and open-water areas.

Stein et al (1996) present detailed IRD data (counts 10 cm^3 > 500 µm) from a series of radiocarbon dated cores on the Scoresby Sund TMF (Fig. 1; PS1726 and PS1730, Fig. 1B) that reflect delivery of coarse sediments in a discrete series of episodes (data from www.Pangaea.de). Stein (2008) noted coarse sediment intervals that were attributed to iceberg-rafting at ~4-15, 16, 17-18, 20-21, and 22-23 ka BP. There are no mineral composition data for PS1730, but data exist for PS2644, which is 300 km away (Table 1, Fig. 1B) (Andrews and Vogt, 2020a; Vogt, 2017). A comparison between PS2644 and #2274 (Fig. 8A) indicates that PS2644, closer to the Scoresby Sund Ice Stream, has more quartz wt% but there are some notable corresponding peaks in both series. However, we note that the quartz wt% were obtained via two different but comparable quantitative methods (Andrews and Vogt, 2020a; Vogt, 2017; Zou, 2016). To evaluate similarities and differences between these two sites we used cross-wavelet analysis (Roesch and Schmidbauer, 2018; Hammer et al., 2001) (Fig. 8). The wavelet analysis of the two quartz records (Fig. 8A) demonstrates both important coeval events as well as obvious differences. In addition, the overall match between these sites for the earlier part of the record adds confidence to our age model, and also emphasizes the important differences between 35 and 65 ka. The reconstructed wavelets for PS2644 show three major pulses of quartz at ~13, 20, and 29 ka BP, and these are matched by much lower peaks at #2274. Conversely, there are no distinct peaks during MIS 3 in PS2644 but there are in #2274. The sense of the directional arrows in Figure 8B is that PS2644 either leads or is in phase with #2274, and there is a hint of a significant shorter period ~60 ka BP with the two records being anti-phase. The cross-wavelet power spectrum (Fig. 8B) confirms the presence of a significant zone of coherence extending from ~10-34 ka BP with the average cross-wavelet power peaking at ~8 ky (Fig. 8C); this is of course similar to the periodicity of HS H-events (see Clark et al., 2007) (e.g. Fig. 3) but lacks the diagnostic carbonate provenance indicators (Andrews and Voelker, 2018). Possibly because of our 0.6 ky sample spacing (Fig. 8A), there is no obvious D-O signal in the quartz PS2644 data, whereas it is evident in the $\delta^{18}O$ *Np* data (Suppl. Fig. 3). The difference in signals between #2274 and PS2644 during MIS 3 (Fig. 8A) suggests a change in either the delivery of quartz-rich sediments or a dampening down of sediment delivery.

The sortable silt evidence indicates that even at the glacial maximum there was flow along the slope in the precursor to the NIJ. As this presently heads toward the Denmark Strait outflow, we suggest that the Nordic Seas acted as a source of deep waters (probably formed in the east where Atlantic inflow continued (Sarnthein et al, 1994)) that overflowed to the North Atlantic where they formed a deep water mass (Howe et al., 2016; Keigwin and Swift, 2017). The classical view of Nordic Sea behaviour during cold periods is that freshwater from melting ice-sheets and -bergs suppresses convection resulting in a severe reduction or even cessation of the AMOC inflow and overflow (e.g. a recent model, including consideration of the EGC, analysing this is from Liu et al, (2018)). However an emerging view is of a slowdown (not cessation) of Nordic Sea overflows in cold periods (Howe et al., 2016; Keigwin and Swift, 2017). A very recent view is that ice discharges in the North Pacific precede Heinrich events and may be implicated as a triggering mechanism (Walczuk et al., 2020). In the Nordic Seas Atlantic water inflow persisted throughout the Pleistocene glacials over the Norwegian slope (Sarnthein et al., 1994; Newton et al., 2018). The evidence here indicates a persistent outflow along the N Iceland Slope with reductions during HS H- events 1, 4, and 6. Flow speed decreases have been noted for both shallow and deep flows in this region during stadials and glacial intervals of the late and mid-Quaternary (Kleiven et al., 2011; McCave and Andrews, 2019b). The Younger Dryas often shows speed decreases but some cores record increased flow (McCave and Andrews, 2019b), as is seen here. These disparities remain a puzzle.

4.2 Rationalizing mineralogical and biomarker proxies for sea ice reconstruction

When detected, the concentrations of IP_{25} and HBI II were mainly much lower than those reported previously for mid-late Holocene (ca. 6-0 cal. ka) and deglacial (ca. 15-11 ka) sites from the NIS (Cabedo-Sanz et al., 2016; Xiao et al., 2017). However, the presence and concentration of IP_{25} at ca. 3.7 ka aligns with previous data reported from core JR51-GC35 (located 76 km SW of #2274 (Figs.1B and 7; Table 1)) for the mid-Holocene (Cabedo-Sanz et al., 2016), consistent with the delivery of drift ice across the NIS at that time (Fig. 7). The otherwise general absence of IP_{25} and HBI II in #2274 points towards an environment unfavorable for sea ice diatom growth, namely ice-free conditions or a setting of near-permanent ice cover. To distinguish between these two scenarios, we measured three other biomarker types indicative of open water conditions, i.e. brassicasterol, HBI III and alkenones. In the case of brassicasterol, a phytosterol characteristic of marine diatoms (Volkman, 1986), concentrations in selected sediments from #2274 were relatively high in the Holocene section and typically two orders of magnitude lower in older (>14 ka) intervals, indicative of much lower glacial primary productivity reflecting near-perennial sea ice cover. Similarly, HBI III, a biomarker derived from certain open water diatoms (Belt et al., 2017), was only detected in Holocene sections (data not shown). Consistent with these findings, concentrations of alkenones derived from coccolithophorid blooming in mid-late summers were also substantially lower in the older sections compared to those in the Holocene (Fig. 6). Further, the relatively high percentage contribution of the tetra-unsaturated alkenone $C_{37:4}$ prior to the Holocene (mean value 36% compared to 6% for the Holocene) is consistent with a dominance of polar waters (Sicre et al., 2002; Bendle et al., 2005) potentially laden with sea ice. Alkenone-derived SST estimates for the Holocene (ca. 7–9°C) are in line with those reported from other high-resolution studies from the NIS (e.g. Bendle and Rosell-Melé, 2007; Sicre et al., 2008b; Kristjansdottir et al. 2016). In contrast, SST estimates prior to the Holocene were somewhat higher (ca. 8–16°C; mean 11.4°C) although the accuracy of such estimates might be lower than for the Holocene owing to the relatively high contributions from $C_{37:4}$ (Bendle and Rosell-Melé, 2004). Anomalously warm SSTs associated with low alkenone concentrations during glacial time have been reported in previous studies and attributed to advection of detrital alkenones (Sicre et al., 2005; Knutz et al., 2011). Such advection by surface currents can introduce significant bias in regions where there are large productivity and SST gradients, thereby overprinting any local signal (Bendle and Rosell-Melé, 2004; Conte et al., 2006). With extremely low alkenone production due to the presence of ice at #2274, transport of allochthonous alkenones within the IC likely explains the deviation in SSTs towards seemingly unrealistic warmer values. In any case, the most robust aspects of the biomarker data point towards near-perennial sea ice cover prior to the Holocene, although the presence of both phytosterols and alkenones (albeit at low concentrations) indicates the occurrence of at least partial open water conditions, potentially restricted to leads or regions of partial ice melt within otherwise heavily consolidated pack ice. Such conditions would likely have led to short-term and reduced primary production during relatively short summer seasons and limited to the near-surface layer due to a strongly-stratified water column resulting from partial ice melt. Both such uppermost surface layer production conditions in leads and advection of allochthonous alkenones within the IC would account for the anomalously high glacial SSTs.

Our conclusion of near-perennial sea ice during MIS 3 and MIS 2 is broadly consistent with outcomes from a recent 120,000 yr reconstruction of sea-ice conditions for the North Atlantic (Maffezzoli et al., 2019) based on the analysis of enriched bromine (Br_{enr}) in an ice core from the Renland Ice Cap (RIC) 560 km WNW from #2274 (Figs. 1 and 7 [RIC]). Albeit at a much broader spatial resolution (i.e. 50-85° N), Maffezzoli et al. (2019) proposed that MIS 3 and MIS 2 experienced a (variable) mix of multi-year and first-year sea ice, before transitioning to mainly first-year ice and open water conditions following the termination of the LGM. Interestingly, the greater range of sea ice cover inferred from the RIC Br_{enr} record is not at all clear in our #2274 record, but is evident in a biomarker record from the eastern Nordic Seas, with extensive/near-perennial sea ice cover during stadials and H-events (i.e. comparable to #2274) but ice-free conditions during interstadials (since ca. 90 ka BP); such differences between marine sites in the western and eastern Nordic Seas presumably reflects the variable influence of warm Atlantic water, limited to the eastern Nordic Seas (Hoff et al., 2016). The most prominent signature of first-year ice in the Br_{enr} records occurred during the Younger Dryas and it is noteworthy that a transition from permanent to increasing seasonal sea ice at the NIS was reported for this interval following a biomarker-based reconstruction of surface oceanographic conditions from core #2272 (Fig. 1; 7; Xiao et al., 2017). Further, based on relatively high concentrations of IP_{25} in MD99-2272 during the Younger Dryas and the preceding Bølling-Allerød, Xiao et al. (2017) concluded that biomarker production was likely associated with locally formed first year ice rather than from advected drift ice, the latter being a feature of modern-day oceanography. In contrast, our new data from #2274 indicate still near-permanent sea ice cover at this time (Fig. 7). As such, we interpret the combined ice core and marine sediment core data to suggest that as climate conditions ameliorated at the end of the LGM, near-permanent sea ice cover transitioned to first-year seasonal sea ice in the southern part of the region, especially during the Bølling-Allerød and Younger Dryas, likely due to increasing influence of the IC (Xiao et al., 2017); however, the spatial extent of this area of first year ice, located southward of the near-permanent sea ice front that characterizes MIS 3 and MIS 2, remains uncertain at this point (see Fig. 7 sub-panel). Large-scale sea ice reduction then characterized the early Holocene (Fig. 7), with a marked increase in all open water primary productivity biomarker proxies (Fig. 6). Increasing drift ice subsequently became a characteristic of the NIS from the mid Holocene onwards (Fig. 7; Cabedo-Sanz et al., 2016).

Conclusions

The multi-proxy sediment data from core #2274 130 km off the north Iceland coast appears at first sight to yield conflicting interpretations depending on whether sediment mineral composition or biomarker proxy data are being considered; however, these can be resolved through a more detailed consideration of the mode(s) of iceberg drift and trajectory through largely consolidated and near-pervasive sea ice. The low- resolution sampling for grain-size restricts detailed interpretation but the sediments are mostly moderately sorted in the silt range allowing a valid record of bottom flow speed. This shows low flow speeds during H-events 1, 4 and 6 related to decrease in Nordic Sea overflow, but not cessation, and a peak in the Younger Dryas.

The mineral composition of the < 2 mm grain-size sediment samples shows 5 peaks with wt% of quartz values significantly higher than Holocene values. The variations in the quartz wt% are also reflected in the estimated contributions of sediment from Precambrian and Caledonian bedrock sources of NE Greenland. These data require sediment transport to the #2274 site during MIS 3 and MIS 2. If the transport is by icebergs then the sea ice cover had to allow icebergs to drift southward, as they do at present (Figs. 1C, 7). A framework of near-permanent sea ice is confirmed from ultra-low seasonal sea ice and open water biomarker concentrations. On the other hand, the occurrence of non-zero concentrations of some phytoplanktic biomarkers, and numbers of near-surface planktonic foraminfera (Table 3) points to some short-term open water conditions, either from limited sea ice melt or following the opening of leads; the presence of drifting icebergs may be significant in this respect (Fig. 7).

An underlying question for HS H-events is whether North Atlantic-wide glacial marine sediment events were triggered as a response to events in Hudson Strait or whether the events are part of a shared response to broader regional oceanographic conditions (e.g. Marcott, et al., 2011; Bassis et al., 2017; Velay-Vitow et al., 2019). Thus, were "coeval" HS H- events on the East Greenland margin (Stein et al., 1996; Andrews et al., 1998; Voelker, 1999), or lagged events (e.g. Baffin Bay: Simon et al., 2014 Jennings et al., 2018), triggered in response to events in the Hudson Strait ice stream? If our quartz and IRD events (Figs. 3 and 8) are indeed coeval with HS H-events, this implies that the stability of ice streams on the NE and E Greenland shelf (and N Iceland) and Hudson Strait may all have been affected by basin-wide subsurface warming in response to a reduction in the Atlantic meridional overturning circulation (Shaffer et al., 2004; Clark et al., 2007; Marcott et al., 2011).

Acknowledgements

We thank Dr Anne E. Jennings for picking and providing the foraminifera for the radiocarbon dates, and Dr Haflidi Haflidasson for the identification and geochemical analysis of the tephra. Professor Grant Bigg provided guidance on the role of icebergs and sea ice. We thank the Centre National de la Recherche Scientifique (CNRS) for MAS salary and the crew of the *RV* Marion Dufresne for coring operations during the IMAGESV cruise. Data from this study will be archived at: www.Pangaea.de, along with other IMAGESV data for MD99-2274. We acknowledge the availability and our use of data from PS1726, PS1730, and PS2644, which we accessed through www.Pangaea.de. Finally, we thank three anonymous reviewers who provided critical and helpful feedback on previous versions of the manuscript.

Tables

Table 1 Location of the cores referenced in this study and showing distance from MD99-2274. Cores located on Fig. 1A and B unless noted as NA. The last 5 sites are cores that specify sediment sources based on radiogenic isotopic data (Verplanck et al., 2009; White et al., 2016).

Table 2 A and B: Data for two possible depth/age models for MD99-2274 used in the Bayesian "Bacon" model—see text. cc = 0 when date derived from other sources and does not require calibration; cc = 2 when ocean reservoir correction $\Delta R = 0$ is used (marine IntelCal 13; Reimer et al., 2013).

Table 3: Depth/age data and calibrated ages for radiocarbon dates on near-surface planktonic foraminifera (see Figs. 1 and 5). Ocean reservoir correction $\Delta R = 0$.

Suppl. Table: Geochemistry of the tephra layer (see text). Courtesy Dr. H. Haflidasson)

Figure Captions

Figure 1: A) location of MD99-2274 and some other cores noted in the paper (Table 1) (ODV, Schlitzer, 2011). The shaded areas represent the late glacial maximum (LGM) extent of the ice sheets north of Denmark Strait; the words "basalt" and "felsic" define the primary sediment mineral sources and the arrows show probable flow paths for icebergs. BB = Blosseville Basi; TMF = Scoresby Sund Trough Mouth Fan; B) Additional cores referenced in the paper (see also Table 1). Note that "Cald" on this figure references the southern outcrop of the Greenland Caledonides (Higgins et al.,

2008). SS = Scoresby Sund; RIC = Renland Ice Cap. C) Surface and bottom currents and historical April sea-ice edge (1870-1920) (dashed white line; Divine and Dick, 2006). NIIC = North Iceland Irminger Current; EGC = East Greenland Current; EIC = East Iceland Current; Yellow lines: Bottom Currents DSOW = Denmark Strait Overflow Water; NIJ = North Iceland Jet., S = Separated East Greenland Current; OC = Iceland Sea Ocean Convection site (after Harden et al., 2016).

Figure 2: A) Downcore plot of magnetic susceptibility (SI^{-5}) and Bayesian ((Blaauw and Christen, 2016) depth age plots for MD99-2274 (see Table 2)---the red curve is for the initial available data blue curve is for the estimated ages with the addition of an estimated core top age and the presence of the Vedde and NAAZII tephras (see text). The Marine Isotope Stage (MIS) boundaries are indicated. Location of radiocarbon dates and tephras are noted. B) Plot of the departures from the median values of magnetic susceptibility ($2.03 * 10^{-3}$ SI) and quartz wt% (5.3). Note that the quartz axis is reversed.

Figure 3: Variation in the Sortable Silt mean size (3-point 1-2-1 weighted smoothing with raw data dots) and IRD% >240 μm. Minima in $\overline{SS}$ are seen at the time of Hudson Strait H events -H6, -H4 and -H1 while -H4, -H2, early -H1 and the YD (-H0) are marked by elevated IRD %. Blue bars are regions where the data are unreliable indicators of flow speed according to the $\overline{SS}$ -SS% correlation criterion of McCave and Andrews, (2019a)

Figure 4: Plots of the variations in the weight% of minerals in MD99-2274, the quartz/pyroxene ratio, and magnetic susceptibility. The green shaded areas represent Holocene values, hence points above represent departures. Numbers 1 through 5 identify IRD quartz peaks. The vertical blue shading areas represent times when the weight% of quartz exceeds Holocene limits.

Figure 5: Plots of the sediment source percentages and the degree of fit (DOF), that is the average absolute bias in the SedUnMix calculation of (observed mineral wt% - predicted mineral weight%) for each sample. The top panel shows the location of measurable quantities of gravel, and sites of tephra layers and the radiocarbon dates on near-surface planktonic foraminifera (Table 3). Numbers on the NE Greenland panel represent the peaks in that source and the yellow bars locate areas with minimal input from that area.

Figure 6: Biomarker data (A) IP_{25} and HBI II concentrations; (B) $\sum C_{37:3}+C_{37:2}$ alkenone and brassicasterol concentrations; C) SST° C estimates and the $\%C_{37:4}$; and D) Weight % quartz and different coarse sediment fractions.

Figure 7: Schematic presentation of changes in sea ice and iceberg distribution. The first panel (upper left) shows core locations (see Table 1 and Fig. 1A and B) and the adjoining panel the inferred conditions during MIS 3 and 2 with pervasive sea ice and embedded icebergs. The remaining panels show the proposed evolution in the state of sea ice and iceberg supply (red triangles) during deglaciation into the Holocene (adapted from

Cabedo-Sanz et al., 2016; Xiao et al., 2017). SS =Scoresby Sound, RIC=Renland Ice Cap.

Figure 8: Analysis of the quartz wt% records from PS2644 (Vogt, 2017) and MD99-2274 at a common 0.6 ky spacing. A) Original quartz data (black line) and the wavelet reconstructions for the two records; B) Cross-wavelet power spectrum of quartz wt% for PS2644 and MD99-2274. The cone of confidence indicated by the light grey areas; 0.05% probability area demarcated by white line. Arrows pointing to the right mean that the two records are in phase, arrows pointing down mean that x leads y, arrows pointing to the left indicate the records are anti-phase and pointing up indicates that #2274 leads PS2644. C) Cross-wavelet (Fig. 8B) average power. The 0.05 significance period is red and delimited by the dashed slanting line. The horizontal dashed line indicates the peak periodicity (~8.5 ky).

Suppl. Figure 1: Data for VM30-130 (see Fig. 1 and Table 3).

Suppl. Figure 2: Showing the reduced major axis association between sortable silt mean size ($\overline{SS}$) and SS%.

Suppl. Figure 3: $\delta^{18}O$ *N. pachyderma* plots of cores from the Blosseville Basin/Scoresby Sund Trough Mouth Fan (see Fig. 1 and 8) from cores PS1730 (Stein et al., 1996a,b, and PS2644 (Voelker, 1999).

References

Aitchison, J., 1986. The statistical analysis of compositional data. Chapman and Hall, London.

Andrews, J.T., Bjork, A.A., Eberl, D.D., Jennings, A.E., Verplanck, E.P., 2015. Significant differences in late Quaternary bedrock erosion and transportation: East versus West Greenland ~ 70°N and the evolution of glacial landscapes. Journal of Quaternary Science 30, 452-463.

Andrews, J.T., Cabedo-Sanz, P., Jennings, A.E., Olafsdottir, S., Belt, S.T., Geirsdottir, A., 2018. Sea ice, ice-rafting, and ocean climate across Denmark Strait during rapid deglaciation (similar to 16-12 cal ka BP) of the Iceland and East Greenland shelves. Journal of Quaternary Science 33, 112-130.

Andrews, J.T., Cooper, T.A., Jennings, A.E., Stein, A.B., Erlenkeuser, H., 1998: Late Quaternary iceberg-rafted detritus events on the Denmark Strait–Southeast Greenland continental slope (∼65°N): related to North Atlantic Heinrich events? Marine Geology 149, 211-228.

Andrews, J.T., Dunhill, G., Vogt, C., Voelker, A.H.L., 2017. Denmark Strait during the Late Glacial Maximum and Marine Isotope Stage 3: Sediment sources and transport processes. Marine Geology 390, 181-198.

Andrews, J.T., Eberl, D.D., 2007. Quantitative mineralogy of surface sediments on the Iceland shelf, and application to down-core studies of Holocene ice-rafted sediments. Journal of Sedimentary Research 77, 469-479.

Andrews, J.T., Eberl, D.D., 2012. Determination of sediment provenance by unmixing the mineralogy of source-area sediments: The "SedUnMix" program. Marine Geology 291, 24-33.

Andrews, J.T., Helgadottir, G., 2003. Late Quaternary ice cap extent and deglaciation of Hunafloaall, NorthWest Iceland: Evidence from marine cores. Arctic, Antarctic, and Alpine Research 35, 218-232.

Andrews, J.T., Jónsdóttir, I., Geirsdóttir, A., 2019. Tracking Holocene drift-ice limits on the NW/SW Iceland shelf: comparing proxy data with observation and historical evidence. Arctic, Antarctic, and Alpine Research. 51, 96-114.

Andrews, J.T., Kristjansdottir, G.B., Eberl, D.D., Jennings, A.E., 2013. A quantitative X-ray diffraction inventory of tephra and volcanic glass inputs into the Holocene marine sediment archives of Iceland: A contribution to V.A.S.T. Polar Research 1-15.

Andrews, J.T., Stein, R., Moros, M., Perner, K., 2016. Late Quaternary changes in sediment composition on the NE Greenland margin (~73 degrees N) with a focus on the fjords and shelf. Boreas 45, 381–397.

Andrews, J.T., Voelker, A., 2018. "Heinrich events" (& sediments): A history of terminology and recommendations for future usage. Quaternary Science Reviews 187, 31-40.

Andrews, J.T., Vogt, C., 2014. Source to Sink: Statistical identification of regional variations in the mineralogy of surface sediments in the western Nordic Seas (58°N – 75°N; 10° W -- 40°W). Marine Geology 357, 151-162.

Andrews, J.T., Vogt, C., 2020a. Variations in felsic- versus mafic-sources in the Western Nordic Seas during MIS 1 to MIS 4 Marine Geology 424, 106164.

Andrews, J.T. and Vogt, C. 2020b: Results of bulk sediment X-ray diffraction analysis and quantification of mineral phases based on the RockJock quantitative analysis. Pangaea. https://doi.pangaea.de/10.1594/PANGAEA.923135

Austin, W.E.N., Hibbert, F.D., 2012. Tracing time in the ocean: a brief review of chronological constraints (60-8 kyr) on North Atlantic marine event-based stratigraphies. Quaternary Science Reviews 36, 28-37.

Bai, Y., Chen, J.F., Sicre, M.-A., Jin, H., Ren, J., Li, H., Xue, B., Ji, Z., Zhuang, Y., Klein, V., Zhao, M., 2019. Seasonal and spatial variability of sea ice and phytoplankton biomarker flux in the Chukchi Sea (Western Arctic). Progress in Oceanography 171, 22-37.

Bassis, J.N., Petersen, S.V. Cathles, L.M., 2017. Heinrich events triggered by ocean forcing and modulated by isostatic adjustment. Nature 542, 332-334.

Belt, S.T., 2018. Source-specific biomarkers as proxies for Arctic and Antarctic sea ice, Organic Geochemistry 125, 277–298, doi: 10.1016/j.orggeochem.2018.10.002.

Belt, S.T., Masse, G., Rowland, S.J., Poulin, M., Michel, C., LeBlanc, B., 2007. A novel chemical fossil of palaeo sea ice: IP_{25}. Organic Gechemistry 38, 16-27.

Belt, S.T., Müller, J., 2013. The Arctic sea ice biomarker IP_{25}: a review of current understanding, recommendations for future research and applications in palaeo sea ice reconstructions. Quaternary Science Reviews 79, 9-25.

Belt, S.T., Cabedo-Sanz, P., Smik, L., Navarro-Rodriguez, A., Berben, S.M. P., Knies, J., Husum, K., 2015. Identification of paleo Arctic winter sea ice limits and the marginal ice zone: optimised biomarker-based reconstructions of late Quaternary Arctic sea ice. Earth and Planetary Science Letters 431, 127-139.

Belt, S.T., Brown, T.A., Smik, L., Tatarek, A., Wiktor, J., Stowasser, G., Assmy, P., Allen, C.A., Husum, K., 2017. Identification of C_{25} highly branched isoprenoid (HBI) alkenes in diatoms of the genus *Rhizosolenia* in polar and non-polar marine phytoplankton. Organic Geochemistry 110, 65–72

Bendle, J., Rosell-Melé, A., 2004. Distributions of UK'_{37} and UK_{37} in the surface waters and sediments of the Nordic Seas: implications for paleoceanography. Geochemistry, Geophysics, Geosystems, Q11013. doi:10.1029/2004GC000741.

Bigg, G.R., 2016. Icebergs. Their Science and links to Global Change. Cambridge University Press.

Blaauw, M., 2012. Out of tune: the dangers of aligning proxy archives. Quaternary Science Reviews 36, 38-49.

Blaauw, M., Christen, J.A., Bacon Manual, 2016. -v2.2, p. 11 pp.

Blaauw, M., Christen, J.A., 2005. The problems of radiocarbon dating. Science 308, 1552-1553.

Boers, N., Ghil, M., Rousseau, D.D., 2018. Ocean circulation, ice shelf, and sea ice interactions explain Dansgaard-Oeschger cycles. Proceedings of the National Academy of Sciences of the United States of America 115, E11005-E11014.

Boers, N., Goswami, B., Ghil, M., 2017. A complete representation of uncertainties in layer-counted paleoclimate archives. Climate of the Past 13, doi:10.5194/cp-13-1169-2017

Brakstad, A., Vage, K., Havik, L., Moore, G.W.K., 2019. Water Mass Transformation in the Greenland Sea during the Period 1986-2016. Journal of Physical Oceanography 49, 121-140.

Brendryen, J., Haflidason, H., Sejrup, H.P., 2011. Non-synchronous deposition of North Atlantic Ash Zone II in Greenland ice cores, and North Atlantic and Norwegian Sea sediments: an example of complex glacial-stage tephra transport. Journal of Quaternary Science 26, 739-745.

Brooks, C.K., Nielsen, T.F.D., 1982. The Phanerozoic development of the Kangerdlugssuaq area, East Greenland. Meddelelser on Gronland, Geoscience 9, 1-30.

Cabedo-Sanz, P., Belt, S.T., Jennings, A.E., Andrews, J.T., Geirsdóttir, Á., 2016. Variability in drift ice export from the Arctic Ocean to the North Icelandic Shelf over the last 8000 years: A multi-proxy evaluation. Quaternary Science Reviews 146, 99-115.

Chayes, F., 1971. Ratio correlation. University of Chicago Press, Chicago.

Clark, D.L., 1990a. Arctic Ocean ice cover; Geologic history and climatic significance, The Geology of North America. Geological Society of America, pp. 53-62.

Clark, D.L., 1990b. Stability of the Arctic Ocean ice-cover and Pleistocene warming events: Outlining the problem, in: Bleil, U., Thiede, J. (Eds.), Geological History of the Polar Oceans: Arctic Versus Antarctic. Kluwer Academic Publishers, Netherlands, pp. 273-287.

Clark, P. U., Hostetler, S. W., Pisias, N. G., Schmittner, A., and Meissner, K. J., 2007. Mechanisms for a ~7 kyr climate and sea-level oscillation during marine isotope stage 3. In Schmittner, A., Chiang, J., and Hemming, S. (eds.), *Ocean Circulation: Mechanisms and Impacts*. Geophysical Monograph 173. Washington, DC: AGU, pp. 209–246.

Conte, M. H., M.-A. Sicre, C. Rühlemann, J. C. Weber, S. Schulte, D. Schulz-Bull, T. Blanz, 2006. Global temperature calibration of the alkenone unsaturation index ($U^{K'}_{37}$) in surface waters and comparison with surface sediments, *Geochemistry, Geophysics, Geosystems* **7**, Q02005, doi:10.1029/2005GC001054.

Darby, D.A., Andrews, J.T., Belt, S.T., Jennings, A.E., Cabedo-Sanz, P., 2017. Holocene cyclic records of ice-rafted debris and sea ice variations on the East Greenland and NW Iceland margins. Antarctic, Arctic, and Alpine Research 49, 649-672.

Darby, D.A., Zimmerman, P., 2008. Ice-rafted detritus events in the Artic during the last glacial interval, and the timing of the Innuitian and Laurentide ice sheet calving events. Polar Research 27, 114-127.

Davies, S.M., Wastegard, S., Rasmussen, T.L., Svensson, A., Johnsen, S.J., Steffensen, J.P., Andersen, K.K., 2008. Identification of the Fugloyarbanki tephra in the NGRIP ice core: a key tie-point for marine and ice-core sequences during the last glacial peroid. Quaternary Science Reviews 23, 409-414.

Divine, D.V., Dick, C., 2006. Historical variability of the sea ice edge position in the Nordic Seas. Journal of Geophysical Research 111, 14pp. doi:10.1029/2004JC002851.

Dokken, T.M., Nisancioglu, K.H., Li, C., Battisti, D.S., Kissel, C., 2013. Dansgaard-Oeschger cycles: Interactions between ocean and sea ice intrinsic to the Nordic seas. Paleoceanography 28, 491-502.

Domack, E.W., Jacobson, E.A., Shipp, S., Anderson, J.B., 1999. Late Pleistocene-Holocene retreat of the West Antarctic Ice-Sheet system in the Ross Sea: Part 2 - Sedimentologic and stratigraphic signature. Geological Society of America Bulletin 111, 1517-1536.

Dowdeswell, J.A., Elverhoi, A., Andrews, J.T., Hebbeln, D., 1999. Asynchronous de-position of ice-rafted layers in the Nordic seas and North Atlantic Ocean. Nature 400, 348–351.

Eberl, D.D., 2003. User guide to RockJock: A program for determining quantitative mineralogy from X-ray diffraction data. United States Geological Survey, Open File Report 03-78, 40 pp, Washington, DC.

Elliot, M., Labeyrie, L., Dokken, T., Manthe, S., 2001. Coherent patterns of ice-rafted debris deposited in the Nordic regions during the last glacial (10-60 ka). Earth and Planetary Science Letters 194, 151–163.

Evans, J., Dowdeswell, J. A., Grobe, H., Niessen, F., Stein, R., Hubberten, H.-W. & Whittington, R. J. 2002: Late Quaternary sedimentation in Kaiser Joseph Fjord and the continental margin of East Greenland. In Dowdeswell, J. A. & O Cofaigh, C. (eds.): Glacier-Influenced Sedimentation on High-Latitude Continental Margins, Special Publication 203, 149–179. The Geological Society of London, London.

Evans, J., Dowdeswell, J. A., Grobe, H., Niessen, F., Stein, R., Hub- berten, H.-W. & Whittington, R. J. 2002: Late Quaternary sedi- mentation in Kejser Joseph Fjord and the continental margin of East Greenland. In Dowdeswell, J. A. &O Cofaigh, C. (eds.): Glacier-Influenced Sedimentation on High-Latitude Continental Margins, 149–179. The Geological Society of London, Special Publication 203, London.

Evans, J., O Cofaigh, C., Dowdeswell, J. A. & Wadhams, P. 2009: Marine geophysical evidence for former expansion and flow of the Greenland Ice Sheet across the north-east Greenland continental shelf. Journal of Quaternary Science 24, 279–293.

Evans, J., Dowdeswell, J. A., Grobe, H., Niessen, F., Stein, R., Hub- berten, H.-W. & Whittington, R. J. 2002: Late Quaternary sedi- mentation in Kejser Joseph Fjord and the continental margin of East Greenland. In Dowdeswell, J. A. & O Cofaigh, C. (eds.): Glacier-Influenced Sedimentation on High-Latitude Continental Margins, 149–179. The Geological Society of London, Special Publication 203, London.

Evans, J., O Cofaigh, C., Dowdeswell, J. A. & Wadhams, P. 2009: Marine geophysical evidence for former expansion and flow of the Greenland Ice Sheet across the north-east Greenland continental shelf. Journal of Quaternary Science 24, 279–293.

Evans, J., Dowdeswell, J. A., Grobe, H., Niessen, F., Stein, R., Hubberten, H.-W. & Whittington, R. J. 2002: Late Quaternary sedi- mentation in Kejser Joseph Fjord and the continental margin of East Greenland. In Dowdeswell, J. A. & O Cofaigh, C. (eds.): Glacier-Influenced Sedimentation on High-Latitude Continental Margins, 149–179. The Geological Society of London, Special Publication 203, London.

Evans, J., O Cofaigh, C., Dowdeswell, J. A. & Wadhams, P. 2009: Marine geophysical evidence for former expansion and flow of the Greenland Ice Sheet across the north-east Greenland continental shelf. Journal of Quaternary Science 24, 279–293.

Funder, S., Goosse, H., Jepsen, H., Kaas, E., Kjaer, K.H., Korsgaard, N.J., Larsen, N.K., Linderson, H., Lysa, A., Moller, P., Olsen, J., Willerslev, E., 2011a. A 10,000-year record of Arctic Ocean sea-ice variability-view from the beach. Science, 333, 747-750.

Funder, S., Kjeldsen, K.K., Kjaer, K.H., O Cofaigh, C., 2011b. The Greenland Ice Sheet during the past 300,000 years: A review. p. 699-713 In, Ehlers, J., Gibbard, P.L., and Hughes, P.D., (Eds), Quaternary Glaciations - Extent and Chronology: A Closer Look. Elsevier, Amsterdam

Greco, M., Jonkers, L., Kretschmer, K., Bijma, J., Kucera, M., 2019. Depth habitat of the planktonic foraminifera *Neogloboquadrina pachyderma* in the northern high latitudes explained by sea-ice and chlorophyll concentrations. Biogeosciences 16, 3425-3437.

Hammer, O, Harper, D.A.T., and Ryan, P.D., 2001. PAST: Paleontological statistics software package for education and data analysis. Palaelontologia Electonica, 4.1.4:1-9. http://palaeo-electronica.org/2001_1/past/issue1_01.htm

Harden, B.E., Pickart, R.S., Valdimarsson, H., Vage, K., de Steur, L., Richards, C., Bahr, F., Torres, D., Borve, E., Jonsson, S., Macrander, A., Osterhus, S., Havik, L., Hattermann, T., 2016. Upstream sources of the Denmark Strait Overflow: Observations from a high-resolution mooring array. Deep-Sea Research Part I-Oceanographic Research Papers 112, 94-112

Hassani, H., 2007. Singular Spectrum Analysis: Methodology and comparison. Journal of Data Science 5, 239-257.

Heinrich, H., 1988. Origin and consequences of cyclic ice rafting in the Northeast Atlantic Ocean during the past 130,000 years. Quaternary Research 29, 143-152.

Hemming, S.R., 2004. Heinrich Events: Massive late Pleistocene detritus layers of the North Atlantic and their global climate imprint. Reviews of Geophysics 42, RG1005/2004.

Henriksen, H., 2008. Geological history of Greenland. Geological Survey of Denmark and Greenland, Copenhagen.

Hesse, R., 2016. Ice-proximal Labrador Sea Heinrich layers: a sedimentological approach. Canadian Journal of Earth Sciences 53, 71-100.

Higgins, A.K., Gilotti, J.A., Smith, P.M., 2008. The Greenland Caledonides. Evolution of the Northeast margin of Laurentia. Geological Society of America, Boulder, CO, p. 368.

Hoff, U., Rasmussen, T.L., Stein, R., Ezat, M.M., Fahl, K., 2016. Sea ice and millennial-scale climate variability in the Nordic seas 90 kyr ago to present. Nature Communications 7. 12247.

Howe, J.N.W., Piotrowski, A.M., Noble, T.L., Mulitza, S., Chiessi, C.M., Bayon, G., 2016. North Atlantic Deep Water production during the Last Glacial Maximum. Nature Commun. 7, 11765. doi: 10.1038/ncomms11765

Jennings, A.E., Andrews, J.T. et al.., 2018. Baffin Bay paleoenvironments in the LGM and HS1: Resolving the ice-shelf question. Marine Geology. 402, 5-16.

Jennings, A.E., Reilly, B., Andrews, J.T., Hogen, K., Walczak, M., Stoner, J., Mix, A.C., Jakobsson, M., 2019. Modern ice shelf facies and Early Holocene counterparts in Petermann Fjord and Northern Nares Strait. (Abstract) International Association of Sedimentologists IAS, Rome.

Jonsson, S., and Valdimarsson, H. 2004. A new path for the Denmark Strait overflow water from the Iceland Sea to Denmark Strait. Geophysical Research Letters 31, 4pp. doi:10.1029/2003GL019214, 012004.

Jonsson, S., Valdimarsson, H., 2005. The flow of Atlantic water to the North Icelandic Shelf and its relation to the drift of cod larvae. ICES Journal of Marine Science 62, 1350-1359.

Jonsson, S., Briem, J., 2003. Flow of Atlantic water west of Iceland and onto the north Atlantic shelf. ICES Marine Science Symposia 219, 326-328.

Keigwin, L.D.,and Swift, S.A., 2017. Carbon isotope evidence for a northern source of deep water in the glacial western North Atlantic. Proceedings of the National Academy of Sciences of the United States of America 114, 2831-2835.

Knudsen, K.-L., Eiriksson, J., 2002. Application of tephrachronology to the timing and correlation of palaeoceanographic events recorded in Holocene and Late Glacial shelf sediments off North Iceland. Marine Geology 191, 165-188.

Konert, M., Vandenberghe, J., 1997. Comparison of laser grain size analysis with pipette and sieve analysis: a solution for the underestimation of the clay fraction. Sedimentology 44, 523-535.

Knudsen, K.-L., Jiang, D., Jansen, E., Eiriksson, J., Heinemeier, J., Seidenkrantz, M.-S., 2003. Environmental changes off North Iceland during the deglaciation and the Holocene: foraminifera, diatoms and stable isotopes. Marine Micropaleontology 953, 1-33.

Knutz, P.C., H. Ebbesen, S. Christiansen**,** M.-A. Sicre, and A. Kuijpers, 2011. The triple stage deglacial retreat of the southern Greenland Ice Sheet driven steps by vigorous Irminger Current, and its significance for the Younger Dryas cooling, *Paleoceanography, 26, PA3204,* doi:10.1029/2010PA002053, 2011

Kristjansdottir, G.B., Stoner, J.S., Gronvold, K., Andrews, J.T., Jennings, A.E., 2007. Geochemistry of Holocene cryptotephras from the North Iceland Shelf (MD99-2269): Intercalibration with radiocarbon and paleomagnetic chronostratigraphies. The Holocene 17, 155-176.

Kristjansson, L., Saemundsson, K., Thorarinsson, S., Saemundsson, K., Thorarinsson, S., Einarsson, P., Bjornsson, S., Simonarson, L., Fridleifsson, I., Jaksobsson, S.P., Bjornsson, H., 1979. Special Issue: Geology of Iceland. Jökull 29, 1-101.

Labeyrie, L., Jansen, E., Cortijo, E., 2003. Les rapports de campagnes a la mer MD114/IMAGES V. Institut Polaire Francais Paul-Emile Victor, Brest.

Labeyrie, L.D. and Cortijo, E. 2005: Physical properties of sediment core MD99-2274. Pangaea. https://doi.org/10.1594/PANGAEA.253605

Lakeman, T.R., Pienkowski, A.J., Nixon, F.C., Furze, M.F.A., Blasco, S., Andrews, J.T., King, E.L., 2018. Collapse of a marine-based ice stream during the early Younger Dryas chronozone, western Canadian Arctic. Geology 46, 211-214.

Larsen, N.K., Levy, L.B., Carlson, A.E., Buizert, C., Olsen, J., Strunk, A., Bjork, A.A. and Skov, D.S. (2018) Instability of the Northeast Greenland Ice Stream over the last 45,000 years. *Nature Communications*, 9.doi: 10.1038/s41467-018-04312-7

Lind, E.W., Lilja, C., Wastegard, S., Pearce, N.J.G., 2016. Revisiting the Borrobol Tephra. Boreas 45, 693-643.

Liu, Y., Hallberg, R., Sergienko, O., Samuels, B.L., Harrison, M., & Oppenheimer, M. 2018. Climate response to the meltwater runoff from Greenland ice sheet: evolving sensitivity to discharging locations. Climate Dynamics, 51, 1733–1751. doi 10.1007/s00382-017-3980-7

Lohne, O.S., Mangerud, J., Birks, H.H., 2013. Precise C-14 ages of the Vedde and Saksunarvatn ashes and the Younger Dryas boundaries from western Norway and their comparison with the Greenland Ice Core (GICC05) chronology. Journal of Quaternary Science 28, 490-500.

Maffezzoli, N., Vallelonga, P., Edwards, R., Saiz-Lopez, A., Turetta, C., Kjaer, H.A., Barbante, C., Vinther, B., Spolaor, A., 2019. A 120 000-year record of sea ice in the North Atlantic? Climate of the Past 15, 2031-2051.

Manley, W.F., Jennings, A.E., 1996. Radiocarbon Date List VIII: Eastern Canadian Arctic, Labrador, Northern Quebec, East Greenland Shelf, Iceland Shelf, and Antarctica. INSTAAR, University of Colorado, p. 163 pp.

Marcott, S.A., Clark, P.U., Padman, L., Klinkhammer, G.P., Springer, S.R. , Liu, Z., , Otto-Bliesner, B.L., Carlson, A.E., Ungerer, A., Padman, J., He, F., Cheng, J. and Schmittner, A., 2011: Ice-shelf collapse from subsurface warming as a trigger for Heinrich events. Proceedings of the National Academy of Sciences of the United States of America 108, 13415-13419

Marshall, N.R., Piper, D.J.W., Saint-Ange, F., Campbell, D.C., 2014. Late Quaternary history of contourite drifts and variations in Labrador Current flow, Flemish Pass, offshore eastern Canada. Geology Marine Letters 34, 457-470. doi:10.1007/s00367-014-0377-z.

Mauritzen, C., 1996. Production of dense overflow waters feeding the North Atlantic across the Greenland-Scotland Ridge. 1. Evidence for a revised circulation scheme. Deep-Sea Research I 43, 769-806.

Massé, G., Rowland, S.J., Sicre, M.-A., Jacob, J., Jansen, E., Belt, S.T., 2008. Abrupt climate changes for Iceland during the last millennium: Evidence from high resolution sea ice reconstructions. Earth and Planetary Science Letters 269, 565–569.

Matthews, I.P., Birks, H.H., Bourne, A.J., Brooks, S.J., Lowe, J.J., Macleod, A., Pyne-O'Donnell, S.D.F., 2011. New age estimates and climatostratigraphic correlations for the Borrobol and Penifiler Tephras: evidence from Abernethy Forest, Scotland. Journal of Quaternary Science 26, 247-252.

McCave, I.N., Andrews, J.T., 2019a. Distinguishing current effects in sediments delivered to the ocean by ice. I. Principles, methods and examples. Quaternary Science Reviews 212, 92-107.

McCave, I.N., Andrews, J.T., 2019b. Distinguishing current effects in sediments delivered to the ocean by ice. II. Glacial to Holocene changes in North Atlantic high latitude upper ocean flows. Quaternary Science Reviews 223, no. 105902, 21pp.

McCave, I.N., Hall, I.R., Bianchi, G.G., 2006. Laser vs settling velocity differences in silt grainsize measurements: estimation of palaeocurrent vigour. Sedimentology 53, 919-928.

McCave, I.N., Manighetti, B. and Robinson, S.G., 1995. Sortable silt and fine sediment size/composition slicing: parameters for palaeocurrent speed and palaeoceanography. Paleoceanography 10, 593-610.

McCave, I.N., Thornalley, D.J.R., Hall, I.R., 2017. Relation of sortable silt grain-size to deep-sea current speeds: Calibration of the 'Mud Current Meter'. Deep-Sea Research Part I 127, 1-12.

McCave, I.N., Syvitski, J.P.M, 1991. Principles and methods of geological particle size analysis, in: Syvitski, J.P.M. (Ed.), Principles, methods and application of particle size analysis. Cambridge University Press, pp. 3-21.

McKay, R., Golledge, N.R., Maas, S., Naish, T., Levy, R., Dunbar, G., Kuhn, G., 2016. Antarctic marine ice-sheet retreat in the Ross Sea during the early Holocene. Geology 44, 7-10.

Millo, C., Sarnthein, M., Erlenkeuser, H., Frederichs, T., 2005. Methane-driven Late Pleistocene delta C-13 minima and overflow reversals in the southwestern Greenland Sea. Geology 33, 873–876.

Moles, J.D., McGarvie, D., Stevenson, J.A., Sherlock, S.C., Abbott, P.M., Jenner, F.E., Halton, A.M., 2019. Widespread tephra dispersal and ignimbrite emplacement from a subglacial volcano (Torfajokull, Iceland). Geology 47, 577-580.

Moros, M., McManus, J., Rasmussen, T., Kuijpers, A., Dokken, T., Snowball, I., Nielsen, T., Jansen, E., 2004. Quartz content and the quartz-to-plagioclase ratio determined by X-ray diffraction: a proxy for ice rafting in the northern North Atlantic? Earth and Planetary Science Letters 218, 389-401.

Newton, A.M.W., Huuse, M., and Brocklehurst, S.H. 2018. A persistent Norwegian Atlantic Current through the Pleistocene glacials. Geophysical Research Letters 45, 5599–5608. https://doi.org/10.1029/2018GL077819

Nam, S.-I., Stein, R., Grobe, H., Hubberten, H., 1995. Late Quaternary glacial/interglacial changes in sediment composition at the East Greenland continental margin and their paleoceanographic implications. Marine Geology 122, 243-262.

Norðdahl, H., Ingolfsson, O., 2015. Collapse of the Icelandic ice sheet controlled by sea-level rise? Arktos, 1 pp 1-18.

O'Cofaigh, C., Taylor, J., Dowdeswell, J.A., Rosell-Mele, A., Kenyon, N.H., Evans, J., Mienert, J., 2002. Geological evidence for sediment reworking on high-latitude continental margins and its implications for palaeoceanography: insights from the Norwegian– Greenland Sea. In: Dowdeswell, J.A., Ó Cofaigh, C. (Eds.), Glacier-influenced sedimentation on high-latitude continental margins. Geological Society London Special Paper, 20. Geological Society, London, pp. 325–348.

Paillard, D., Labeyrie, L., Yiou, P., 1996. Macintosh program performs time-series analysis. EOS 77, 379.

Patton, H., Hubbard, A., Bradwell, T., Schomacker, A., 2017. The configuration, sensitivity and rapid retreat of the Late Weischelian Icelandic Ice Sheet. Earth-Science Reviews 166, 223-245.

Petersen, S.V., Schrag, D.P., Clark, P.U., 2013. A new mechanism for Dansgaard-Oeschger cycles. Paleoceanography 28, 24-30.

Phillips, R.L., Grantz, A., 2001. Regional variations in provenance and abundance of ice-rafted clasts in Arctic Ocean sediments: implications for the configuration of late Quaternary oceanic and atmospheric circulation in the Arctic. Marine Geology 172, 91-115.

Pickart, R.S., Torres, D.J., Fratantoni, P.S., 2005. the East Greenland spill jet. Journal of Physical Oceanography 35, 1037-1053.

Prahl, F.G., Muelhausen, L.A., Zahnle, D.L., 1988, Further evaluation of long-chain alkenones as indicators of paleoceanographic conditions. Geochimica et Cosmochmicia Acta 52, 2303-2310.

Rasmussen, S.O., Bigler, M., Blockley, S.P., Blunier, T., Buchardt, S.L., Clausen, H.B., Cvijanovic, I., Dahl-Jensen, D., Johnsen, S.J., Fischer, H., Gkinis, V., Guillevic, M., Hoek, W.Z., Lowe, J.J., Pedro, J.B., Popp, T., Seierstad, I.K., Steffensen, J.P., Svensson, A.M., Vallelonga, P., Vinther, B.M., Walker, M.J.C., Wheatley, J.J., Winstrup, M., 2014. A stratigraphic framework for abrupt climatic changes during the Last Glacial period based on three synchronized Greenland ice-core records: refining and extending the INTIMATE event stratigraphy. Quaternary Science Reviews 106, 14-28.

Rasmussen, T.L., Wastegard, S., Kuijpers, A., van Weering, T.C.E., Heinemeier, J., Thomsen, E., 2003. Stratigraphy and distribution of tephra layers in marine sediment cores from the Faeroe Islands, North Atlantic. Marine Geology 199, 263-277.

Reeh, N., 2004. Holocene climate and fjord glaciations in Northeast Greenland: implications for IRD deposition in the North Atlantic. Sedimentary Geology 165, 333-342.

Reeh, N., Mayer, C., Miller, H., Thomsen, H.H., Weidick, A., 1999. Present and past climate control on fjord glaciations in Greenland: Implications for IRD-deposition in the sea. Geophysical Research Letters 26, 1039-1042.

Reimer, P.J., Bard, E., Bayliss, A., Beck, J.W., Blackwell, P.G., Bronk Ramsey, C., Grootes, P.M., Guilderson, T.P., Haflidason, H., Hajdas, I., Hatt?, C., Heaton, T.J., Hoffmann, D.L., Hogg, A.G., Hughen, K.A., Kaiser, K.F., Kromer, B., Manning, S.W., Niu, M., Reimer, R.W., Richards, D.A., Scott, E.M., Southon, J.R., Staff, R.A., Turney, C.S.M. and van der Plicht, J. (2013) IntCal13 and Marine13 Radiocarbon Age Calibration Curves 0-50,000 Years cal BP. *Radiocarbon*, 55, 1869-1887.

Robinson, S.G., Maslin, M.A., McCave, I.N., 1995. Magnetic susceptibility variations in Upper Pleistocene deep-sea sediments of the N.E. Atlantic: Implications for ice rafting and palaeocirculation at the Last Glacial Maximum. Paleoceanography 10, 221-250.

Roesch, A. and Schmidbauer, H.W.C., 2018: WaveletComp: Computational Wavelet Analysis. R package 1.1. https//CRAN.R-project.org/package=Wavelet.Comp.

Ruddiman, W.F., McIntyre, A., 1981. The North Atlantic Ocean during the last deglaciation. Palaeogeography, Palaeoclimatology, Palaeoecology 35, 145-214.

Sarnthein, M., Winn, K., Jung, S., Duplessy, J. C., Labeyrie, L., Erlenkeuser, H., and Ganssen, G., 1994. Changes in East Atlantic deepwater circulation over the last 30,000 years – An eight-time-slice record. Paleoceanography 9, 209–267.

Sarnthein, M., Pflaumann, U., Weinelt, M., 2003. Past extent of sea ice in the northern North Atlantic inferred from foraminiferal paleotemperature estimates. Paleoceanography 18, doi:10.1029/2002PA000771.

Schlitzer, R., 2011. Ocean Data View, http://odv.awi.de,2011

Sejrup, H.P., Sioholm, J., Furnes, H., Beyer, I., Eide, L., Jansen, E., Mangerud, J., 1989. Quaternary tephrachronology on the Iceland Plateau, north of Iceland. Journal of Quaternary Science 4, 109-114.

Shaffer, G., S.M. Olsen, and C.J. Bjerrum, 2004. Ocean subsurface warming as a mechanism for coupling Dansgaard-Oeschger climate cycles and ice-rafting events. Geophysical Research Letters 31, L24202, doi:10.1029/2004GL020968.

Sicre, M.-A., Bard, E., Ezat, U., Rostek, F., 2002. Alkenone distributions in the North Atlantic and Nordic sea surface waters. Geochemistry, Geophysics, Geosystems, Article 2001GC000159.

Sicre, M.-A., Labeyrie, L., Ezat, U., Duprat, J., Turon, J-L, Schmidt, S., Michel, E., Mazaud A., 2005. Southern Indian Ocean response to Northern Hemisphere Heinrich events. Earth and Planetary Science Letters 240, 724-731, doi: 10.1016.

Sicre, M.-A., Jacob, J., Ezat, U., Rousse, S., Kissel, C., Yiou, P., Eiriksson, J., Knudsen, K.-L., Jansen, E., Turon, J.-L., 2008a. Decadal variability of sea surface temperatures off North Iceland over the last 2000 years. Earth and Planetary Science Letters 268, 137-142.

Sicre, M-A., Yiou, P., Eiriksson, J., Ezat, U., Guimbaut, E., Dahhaoui, I., Knudsen, K.-L., Jansen, E., Turon, J.-L., 2008b. A 4500-year reconstruction of sea surface temperature variability at decadal time scales off North Iceland. Quaternary Science Reviews 27, 2041-2047.

Simon, Q., Hillaire-Marcel, C., St-Onge, G., Andrews, J.T., 2014. North-eastern Laurentide, western Greenland and southern Innuitian ice stream dynamics during the last glacial cycle. Journal of Quaternary Science 29, 14-26.

Skinner L.C. & I.N. McCave. Analysis and modelling of the behaviour of gravity and piston corers based on soil mechanical principles. Marine Geology 199, 181-204.

Skinner, L. C., Muschitiello, F., & Scrivner, A. E., 2019. Marine reservoir age variability over the last deglaciation: Implications for marine carbon cycling and prospects for regional radiocarbon calibrations. Paleoceanography and Paleoclimatology 34, 1807–1815. https://doi.org/10.1029/2019PA003667

Stefansson, U., 1962. North Icelandic Waters. Rit Fiskideildar III. Bind, Vol 3, 269.

Stein, R., 2008. Arctic Ocean Sediments. Processes, Proxies, and Paleoenvironment. Elsevier, New York.

Stein, R., Nam, S.-I., Grobe, H., Hubberten, H., 1996a. Late Quaternary glacial history and short-term ice-rafted debris fluctuations along the East Greenland continental margin, in: Andrews, J.T., Austin, W.A., Bergsten, H., Jennings, A.E. (Eds.), Late Quaternary paleoceanography of North Atlantic margins. Geological Society, London, pp. 135-151.

Stein, R., Nam, S.-Il., Grobe, H., Hubberten, Hans-Wolfgang, H., 1996b. Sedimentology and stable isotope ratios of cores from the East Greenland continental margin. *PANGAEA*, https://doi.org/10.1594/PANGAEA.733965,

Stokes, C.R., Clark, C.D., Darby, D.A., Hodgson, D.A., 2005. Late Pleistocene ice export events into the Arctic Ocean from the M'Clure Strait Ice Stream, Canadian Arctic Archipelago. Global and Planetary Change 49, 139-162.

Telford, R.J., Heegaard, E., Birks, H.J.B., 2003. All age-depth models are wrong: but how badly? Quaternary Science Reviews 23, 1-5.

Trachsel, M., Telford, R.J., 2017 All age-depth models are wrong, but are getting better. Holocene 27, 860-869

van Kreveld, S., Sarthein, M., Erlenkeuser, H., Grootes, P., Jung, S., Nadeau, M.J., Pflaumann, U., Voelker, A., 2000. Potential links between surging ice sheets, circulation changes, and the Dansgaard-Oeschger cycles in the Irminger Sea, 60-18 ka. Paleoceanography 15, 425-442.

Vasskog, K., Langebroek, P.M., Andrews, J.T., Nilsen, J.E.O., Nesje, A., 2015. The Greenland Ice Sheet during the last glacial cycle: Current ice loss and contribution to sea-level rise from a palaeoclimatic perspective. Earth-Science Reviews 150, 45-67.

Velay-Vitow, J., Peltier, W.R., and Stuhne, G. , 2019. Tides of the Glacial Ocean and their role in Heinrich Event instability. Geophysical Research Abstracts. 21, EGU2019-3733.

Venkatesh, S., Murphy, D.L., Wright, G.F., 1994. On the deterioration of icebergs in the marginal ice-zone. Atmosphere-Ocean 32, 469-484.

Verplanck, E.P., Farmer, G.L., Andrews, J., Dunhill, G., Millo, C., 2009. Provenance of Quaternary glacial and glacimarine sediments along the southeast Greenland margin. Earth and Planetary Science Letters 286, 52-62.

Voelker, A.H.L., 1999. Zur Deutung der Dansgaard-Oeschger Ereignisse in ulta-hochauflosenden Sedimentprofilen aus dem Europaischen Nordmeer, Dansgaard-Oeschger events in ultra-high resolution sediment records from the Nordic Seas. Universitat Kiel, Kiel, p. 271.

Voelker, A.H.L., Grootes, P.M., Nadeau, M-J., and Sarnthein, M., 2000. Radiocarbon levels in the Iceland Sea from 25–53 kyr and their link to the earth's magnetic field intensity. Radiocarbon 42, p 437–452

Voelker, A.H.L., Haflidason, H., 2015. Refining the Icelandic tephrachronology of the last glacial period - The deep-sea core P52644 record from the southern Greenland Sea. Global and Planetary Change 131, 35-62.

Voelker, A.H.L., Sarnthein, M., Grootes, P.M., Erlenkeuser, H., Laj, C., ,Mazaud, A., Nadeau, M-J., Schleicher, M., 1998: Correlation of marine 14C ages from the Nordic Seas with the GISP2 isotope record: implications for 14C calibration beyond 25 ka BP. Radiocarbon 40, 517-534.

Volkman, J.K., 1986. A review of sterol markers for marine and terrigenous organic matter. Organic Geochemistry 9, 83–99.

Vogt, C., 2017. Bulk mineral assemblage via Quantitative Phase Analysis with X-ray diffraction of sediment core PS2644-5 KAL. PANGAEA. https://doi.org/10.1594/PANGAEA.875919

Walczuk, M.H. & 13 others, 2020. Phasing of millennial-scale climate variability in the Pacific and Atlantic oceans. Science, 370, 716–720.

Watkins, S.J., Maher, B.A., 2003. Magnetic characterization of present-day deep-sea sediments and sources in the North Atlantic. Earth and Planetary Science Letters 214, 379-394.

White, L.F., Bailey, I., Foster, G.L., Allen, G., Kelley, S.P., Andrews, J.T., Hogan, K., Dowdeswell, J.A., Storey, C.D., 2016. Tracking the provenance of Greenland-sourced, Holocene aged, individual sand-sized ice-rafted debris using the Pb-isotope compositions of feldspars and Ar-40/Ar-39 ages of hornblendes. Earth and Planetary Science Letters 433, 192-203.

Xiao, X., Fahl, K., Stein, R., 2013. Biomarker distributions in surface sediments from the Kara and Laptev seas (Arctic Ocean): indicators for organic-carbon sources and sea-ice coverage. Quaternary Science Reviews 79, 40–52.

Xiao, X., Zhao, M., Knudsen, K.L., Sha, L., Eiríksson, J., Gudmundsdóttir, E., Jiang, H., Guo, Z., 2017. Deglacial and Holocene sea–ice variability north of Iceland and response to ocean circulation changes. Earth and Planetary Science Letters 472, 14–24.

Zou, H., 2016. An X-Ray Diffraction Approach: Bulk Mineral Assemblages as Provenance Indicator of Sediments from the Arctic Ocean. University of Bremen, Bremen, pp. 116. https://elib.suub.uni-bremen.de/edocs/00105354-1.pdf.

Methods

Magnetic susceptibility: Magnetic susceptibility was measured on-board the *Marion Dufresne* (Labeyrie and Cort, 2005) in 2-cm increments (hence ~150yr sampling on average). Measurements were taken on the 1.5 m core sections. In this area of Iceland, the marine deposits are strongly affected by erosion and transport of basalt, which results in very high values of magnetic susceptibility. The export of sediments from the erosion of bedrock with much lower magnetic susceptibilities, such as granites and other felsic-rich bedrock in NE Greenland and from more distant sources (Verplanck et al., 2009; White et al., 2016) will lower the magnetic susceptibility readings. It is important to note that although magnetic susceptibility is straightforward to measure, data interpretation is complex, being a product of sediment density, grain-size, and mineralogy (Robinson et al., 1995; Stoner and Andrews, 1999; Watkins and Maher, 2003).

Quantitative X-ray Diffraction (qXRD): The weight % (wt%) of the non-clay and clay mineral composition of the < 2 mm sediment fractions is based on the US Geological Survey method (Eberl, 2003), which has been used extensively in this region (e.g. Andrews et al., 2017; Andrews and Eberl, 2007; Andrews and Vogt, 2014). One gram of sediment (dry weight) is spiked with 0.111 g of zincite, prepared (Eberl, 2003), run in the X-ray diffractometer, and the resulting intensity data processed in the Excel macro-program Rockjock v6. We investigate the wt% and presence/absence of 34 minerals and reduced this number by combining individual mineral wt% into larger groups, such as k-feldspars, plagioclase, dolomite, and amorphous minerals. Importantly in the context of this paper we had earlier shown that qXRD can recognize the presence of tephra and volcanic glass, with some ability to distinguish between basaltic and rhyolithic glass (Andrews et al., 2013).

To gain a better understanding of possible changes in the provenance of the mineral compositions we processed the mineral wt% data in a sediment unmixing program "SedUnMix" (Andrews and Eberl, 2012). Two models were considered, the first with qXRD results from #2274 with four appropriate bedrocks, namely: basalt, dolerite, gneiss, and granite; and secondly with the mineral compositions of glacial marine sediment samples from potential source areas, namely: NE Greenland, E. Greenland, and Iceland (Suppl. Table of bedrock and marine sediment sources). The program calculates a "degree of fit" and also derives error estimates on each source within a sample. Ideally, the sum of the sources should equal 100% but marked deviations from this suggest that one or more sources have not been included, and/or that the sources are not representative of the sediment samples.

Grain-size: Sediment was wet-sieved at 2 mm and the grain-size volume percentages in 96 intervals between 0.01 and 2000 μm were obtained via a Malvern laser system. Comparisons between the Malvern and other grain-size systems have been documented and found comparable (McCave et al., 2006; McCave and Syvitski, 1991). However, the objections of McCave et al. (2006) to laser sizers on the grounds of grain shape (Konert and Vandenberghe, 1997) are not valid for equant grains such as those produced by glacial grinding, as pointed out by Piper (Marshall et al., 2014), and thus size data are believed valid in the setting of MD2274. Grain-size curves have provided vital information on sediment transport and deposition in this region, and methods have been developed to reconstruct variations in bottom current speed for sediments delivered to the ocean from dominantly glacial sources (McCave and Andrews, 2019a, b) The calibration of sortable silt mean (mean of 10-63 µm), a sensitivity, by McCave et al., (2017) has been applied to changes in the grainsize record.

Biomarkers: Biomarkers were extracted from freeze-dried subsamples (~2-4 g). Prior to extraction, samples were spiked with an internal standard (9-octylheptadec-8-ene, 9-OHD, 10 µL; 10 µg mL^{-1}) to permit quantification of the highly branched isoprenoid (HBI) biomarkers IP_{25}, HBI II and HBI III. 5α-androstan-3β-ol; (0.1 µg) was also added to permit quantification of brassicasterol in some cases. Samples were then saponified in a methanolic KOH solution (~5 mL H_2O:MeOH (1:9); 5% KOH) for 60 min (70 °C). Hexane (3×2 mL) was added to the saponified mixtures, with supernatant solutions, containing non-saponifiable lipids (NSLs), transferred by glass pipettes to glass vials, and solvent removed using a gentle stream of N_2. Dried NSLs were re-suspended in hexane (0.5 mL) and fractionated using column chromatography (SiO_2; 0.5 g). Non-polar lipids, including IP_{25} and HBI II, were eluted with hexane (6 mL), while more polar lipid fractions containing alkenones were eluted with MeOH (6 mL). For a few horizons, additional NSLs were fractionated to yield non-polar (hexane; 6 mL) and polar fractions containing sterols (hexane:methyl acetate 4:1; 6 mL). Each non-polar fraction was further purified to remove saturated components using silver-ion chromatography (Belt et al., 2015), with saturated compounds eluted with hexane (2 mL) and unsaturated compounds, including IP_{25} and other HBIs, collected in a subsequent acetone fraction (3 mL). Analysis of fractions containing IP_{25} and other HBIs was carried out using gas chromatography–mass spectrometry (GC–MS) following the methods and operating conditions described prevously (Belt et al., 2012). Mass spectrometric analysis was carried out in total ion current (TIC) and selected ion monitoring (SIM) modes. The identification of IP_{25} and HBI II was based on their characteristic GC retention indices (e.g. RI_{HP5MS} = 2081,2082 and 2044 for IP_{25}, HBI II and HBI III, respectively) and mass spectra (Belt, 2018). Quantification of all HBIs was achieved by comparison of mass spectral responses of selected ions (e.g. IP_{25}, *m/z* 350; HBI II, *m/z* 348; HBI III, *m/z* 346) in SIM mode with those of the internal standard (9-OHD, *m/z* 350) and normalized according to their respective instrumental response factors, derived from solutions of known biomarker concentration, and sediment masses (Belt et al., 2012). Fractions containing sterols were derivatized with N,O-bis(trimethylsilyl)trifluoroacetamide (BSTFA; 100 μL; 70°C for 60 min) immediately prior to analysis by GC–MS. Sterols were identified by comparison with GC–MS responses compared to those of standards. Sterol quantification was achieved as per the approach described above for HBIs.

Polar factions containing alkenones obtained from elution with MeOH (6 mL) were further purified with 2 mL of hexane:methyl acetate (95:5 v/v) and 2 mL of hexane:methyl acetate (90:10 v/v). Alkenones were analyzed using a Thermo Trace GC Ultra gas chromatograph equipped with a CPSil5 capillary column (50m length, 0.32 i.d. and 0.25 mm film thickness), an FID detector and a septum programmable injector (SPI). Helium was used as carrier gas. 5α-cholestane was added as an external standard prior to GC injection. SST estimates were determined using the following equation (Prahl et al., 1988).

$$U_{37}^{K'} = \frac{C_{37:2}}{C_{37:2} + C_{37:3}} = 0.034\,T + 0.039$$

References for Methods

Andrews, J.T., Dunhill, G., Vogt, C., Voelker, A.H.L., 2017. Denmark Strait during the Late Glacial Maximum and Marine Isotope Stage 3: Sediment sources and transport processes. Marine Geology 390, 181-198.

Andrews, J.T., Eberl, D.D., 2007. Quantitative mineralogy of surface sediments on the Iceland shelf, and application to down-core studies of Holocene ice-rafted sediments. Journal of Sedimentary Research 77, 469-479.

Andrews, J.T., Eberl, D.D., 2012. Determination of sediment provenance by unmixing the mineralogy of source-area sediments: The "SedUnMix" program. Marine Geology 291, 24-33.

Andrews, J.T., Vogt, C., 2020. Variations in felsic- versus mafic-sources in the Western Nordic Seas during MIS 1 to MIS 4 Marine Geology 424, 106164.

Belt, S.T., 2018. Source-specific biomarkers as proxies for Arctic and Antarctic sea ice, Organic Geochemistry 125, 277–298, doi: 10.1016/j.orggeochem.2018.10.002.

Belt, S.T., Brown, T.A., Navarro-Rodriguez, A., Cabedo-Sanz, P., Tonkin, A., Ingle, R., 2012. A reproducible method for the extraction, identification and quantification of the Arctic sea ice proxy IP_{25} from marine sediments. Analytical Methods 4, 705–713.

Belt, S.T., Cabedo-Sanz, P., Smik, L., Navarro-Rodriguez, A., Berben, S.M. P., Knies, J., Husum, K., 2015. Identification of paleo Arctic winter sea ice limits and the marginal ice zone: optimised biomarker-based reconstructions of late Quaternary Arctic sea ice. Earth and Planetary Science Letters 431, 127-139.

Eberl, D.D., 2003. User guide to RockJock: A program for determining quantitative mineralogy from X-ray diffraction data. United States Geological Survey, Open File Report 03-78, 40 pp, Washington, DC.

Konert, M., Vandenberghe, J., 1997. Comparison of laser grain size analysis with pipette and sieve analysis: a solution for the underestimation of the clay fraction. Sedimentology 44, 523-535.

Marshall, N.R., Piper, D.J.W., Saint-Ange, F., Campbell, D.C., 2014. Late Quaternary history of contourite drifts and variations in Labrador Current flow, Flemish Pass, offshore eastern Canada. Geology Marine Letters 34, 457-470. doi:10.1007/s00367-014-0377-z.

McCave, I.N., Andrews, J.T., 2019a. Distinguishing current effects in sediments delivered to the ocean by ice. I. Principles, methods and examples. Quaternary Science Reviews 212, 92-107.

McCave, I.N., Andrews, J.T., 2019b. Distinguishing current effects in sediments delivered to the ocean by ice. II. Glacial to Holocene changes in North Atlantic high latitude upper ocean flows. Quaternary Science Reviews 223, no. 105902, 21pp.

McCave, I.N., Hall, I.R., Bianchi, G.G., 2006. Laser vs settling velocity differences in silt grainsize measurements: estimation of palaeocurrent vigour. Sedimentology 53, 919-928.

McCave, I.N., Manighetti, B. and Robinson, S.G., 1995. Sortable silt and fine sediment size/composition slicing: parameters for palaeocurrent speed and palaeoceanography. Paleoceanography 10, 593-610.

McCave, I.N., Thornalley, D.J.R., Hall, I.R., 2017. Relation of sortable silt grain-size to deep-sea current speeds: Calibration of the 'Mud Current Meter'. Deep-Sea Research Part I 127, 1-12.

McCave, I.N., Syvitski, J.P.M, 1991. Principles and methods of geological particle size analysis, in: Syvitski, J.P.M. (Ed.), Principles, methods and application of particle size analysis. Cambridge University Press, pp. 3-21.

Robinson, S.G., Maslin, M.A., McCave, I.N., 1995. Magnetic susceptibility variations in Upper Pleistocene deep-sea sediments of the N.E. Atlantic: Implications for ice rafting and palaeocirculation at the Last Glacial Maximum. Paleoceanography 10, 221-250.

Stoner, J.S., Andrews, J.T., 1999. The North Atlantic as a Quaternary magnetic archive, in: Maher, B., Thompson, R. (Eds.), Quaternary Climates, Environments and Magnetism. Cambridge University Press, Cambridge, UK, pp. 49-80.

Verplanck, E.P., Farmer, G.L., Andrews, J., Dunhill, G., Millo, C., 2009. Provenance of Quaternary glacial and glacimarine sediments along the southeast Greenland margin. Earth and Planetary Science Letters 286, 52-62.

Watkins, S.J., Maher, B.A., 2003. Magnetic characterization of present-day deep-sea sediments and sources in the North Atlantic. Earth and Planetary Science Letters 214, 379-394.

White, L.F., Bailey, I., Foster, G.L., Allen, G., Kelley, S.P., Andrews, J.T., Hogan, K., Dowdeswell, J.A., Storey, C.D., 2016. Tracking the provenance of Greenland-sourced, Holocene aged, individual sand-sized ice-rafted debris using the Pb-isotope compositions of feldspars and Ar-40/Ar-39 ages of hornblendes. Earth and Planetary Science Letters 433, 192-203.

Figures with Captions

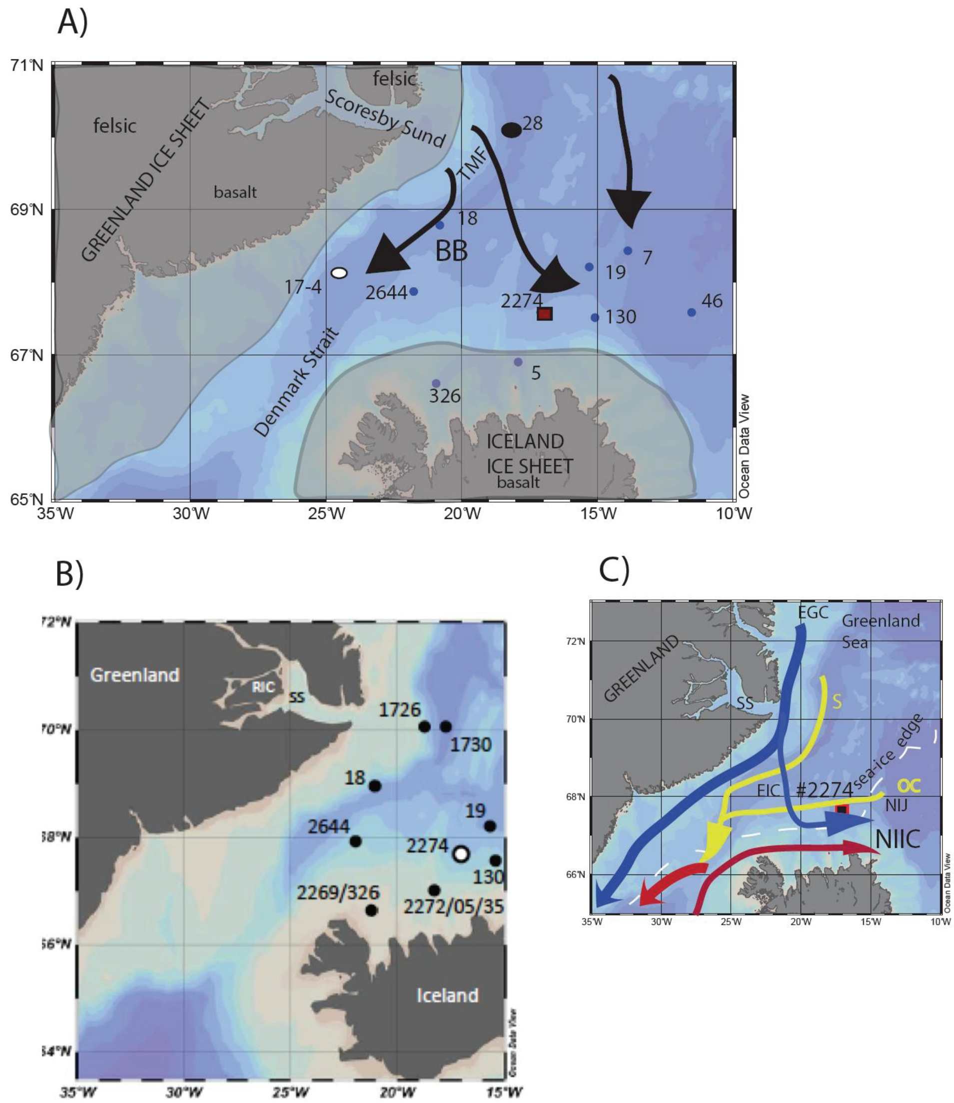

Figure 1: A) location of MD99-2274 and some other cores noted in the paper (Table 1) (ODV, Schlitzer, 2011). The shaded areas represent the late glacial maximum (LGM) extent of the ice sheets north of Denmark Strait; the words “basalt” and “felsic” define the primary sediment mineral sources and the arrows show probable flow paths for icebergs. BB = Blosseville Basi; TMF = Scoresby Sund Trough Mouth Fan; B) Additional cores referenced in the paper (see also Table 1). Note that “Cald” on this figure references the southern outcrop of the Greenland Caledonides (Higgins et al., 2008). SS = Scoresby Sund; RIC = Renland Ice Cap. C) Surface and bottom currents and historical April sea-ice edge (1870-1920) (dashed white line; Divine and Dick, 2006). NIIC = North Iceland Irminger Current; EGC = East Greenland Current; EIC = East Iceland Current; Yellow lines: Bottom Currents DSOW = Denmark Strait Overflow Water; NIJ = North Iceland Jet., S = Separated East Greenland Current; OC = Iceland Sea Ocean Convection site (after Harden et al., 2016).

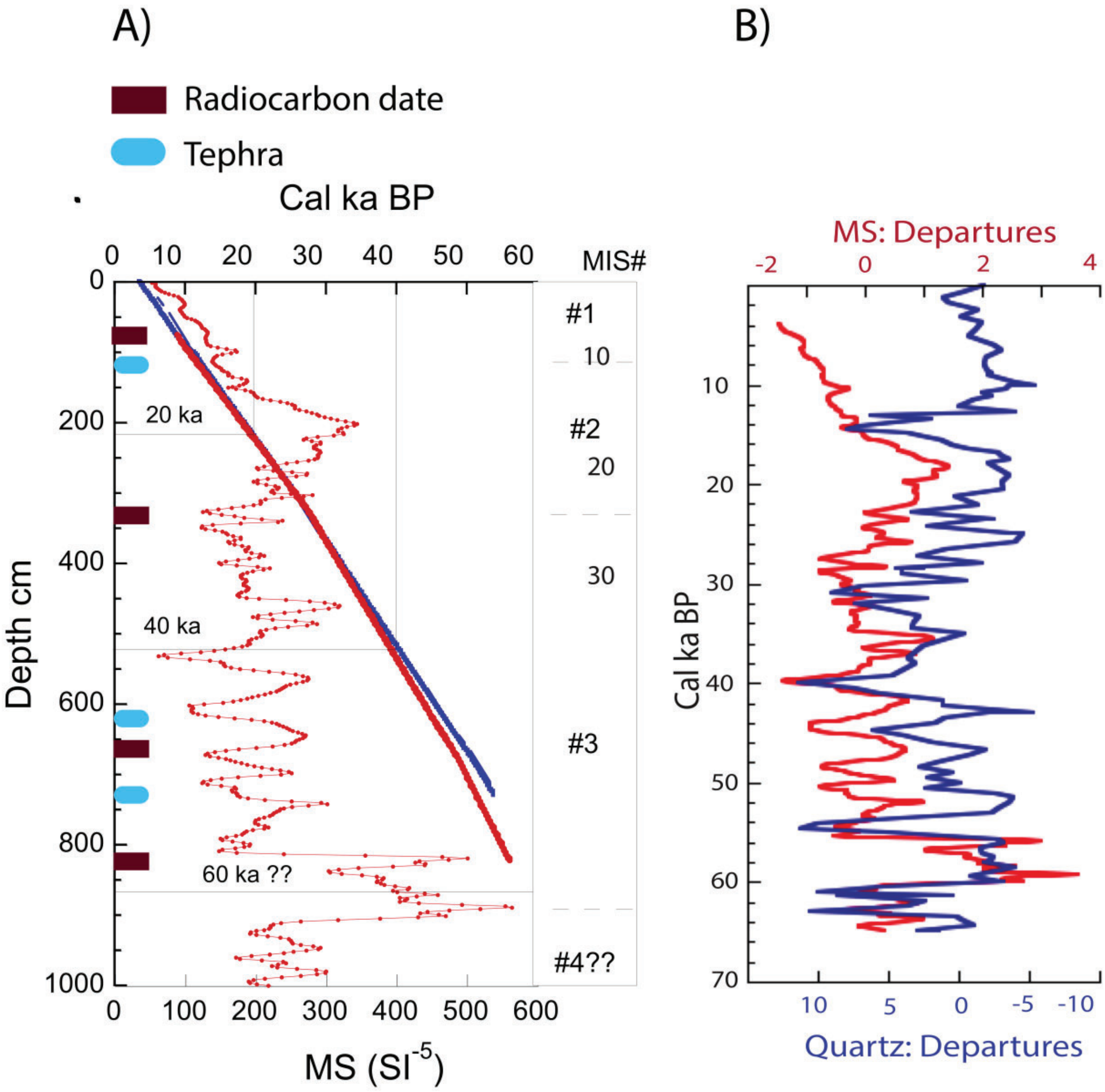

Figure 2: A) Downcore plot of magnetic susceptibility (SI^{-5}) and Bayesian ((Blaauw and Christen, 2016) depth age plots for MD99-2274 (see Table 2)---the red curve is for the initial available data blue curve is for the estimated ages with the addition of an estimated core top age and the presence of the Vedde and NAAZII tephras (see text). The Marine Isotope Stage (MIS) boundaries are indicated. Location of radiocarbon dates and tephras are noted. B) Plot of the departures from the median values of magnetic susceptibility ($2.03 * 10^{-3}$ SI) and quartz wt% (5.3). Note that the quartz axis is reversed.

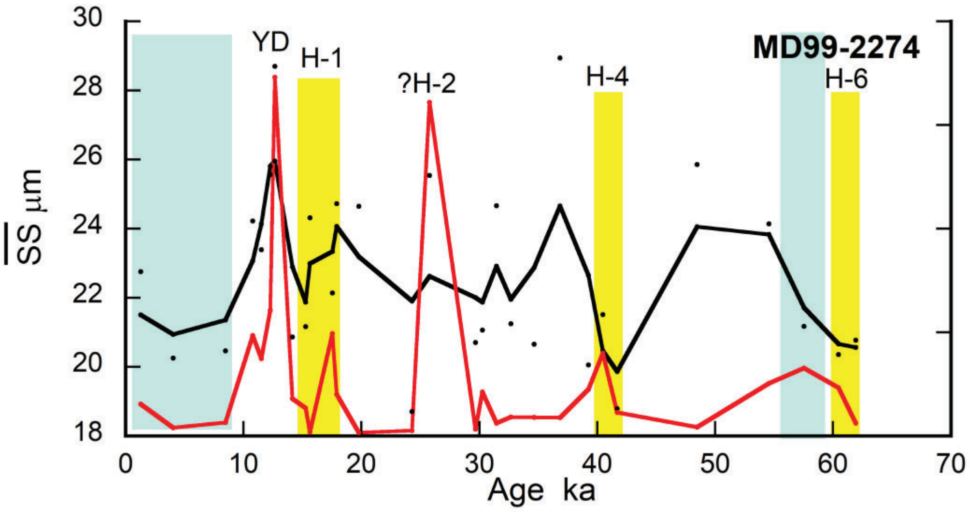

Figure 3: Variation in the Sortable Silt mean size (3-point 1-2-1 weighted smoothing with raw data dots) and IRD% >240 µm. Minima in $\overline{SS}$ are seen at the time of Hudson Strait H events -H6, -H4 and -H1 while -H4, -H2, early -H1 and the YD (-H0) are marked by elevated IRD %. Blue bars are regions where the data are unreliable indicators of flow speed according to the $\overline{SS}$ -SS% correlation criterion of McCave and Andrews, (2019a)

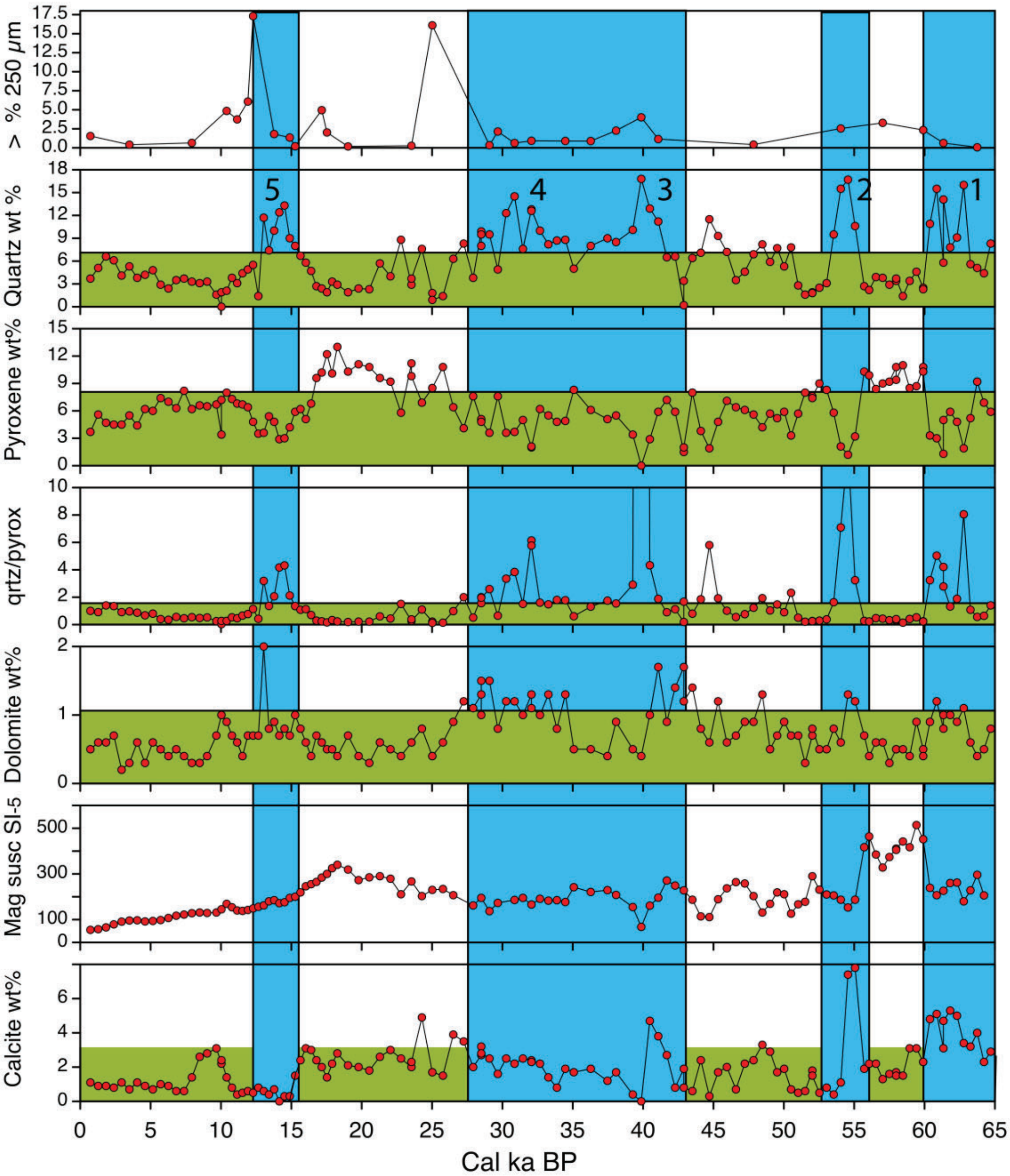

Figure 4: Plots of the variations in the weight% of minerals in MD99-2274, the quartz/pyroxene ratio, and magnetic susceptibility. The green shaded areas represent Holocene values, hence points above represent departures. Numbers 1 through 5 identify IRD quartz peaks. The vertical blue shading areas represent times when the weight% of quartz exceeds Holocene limits.

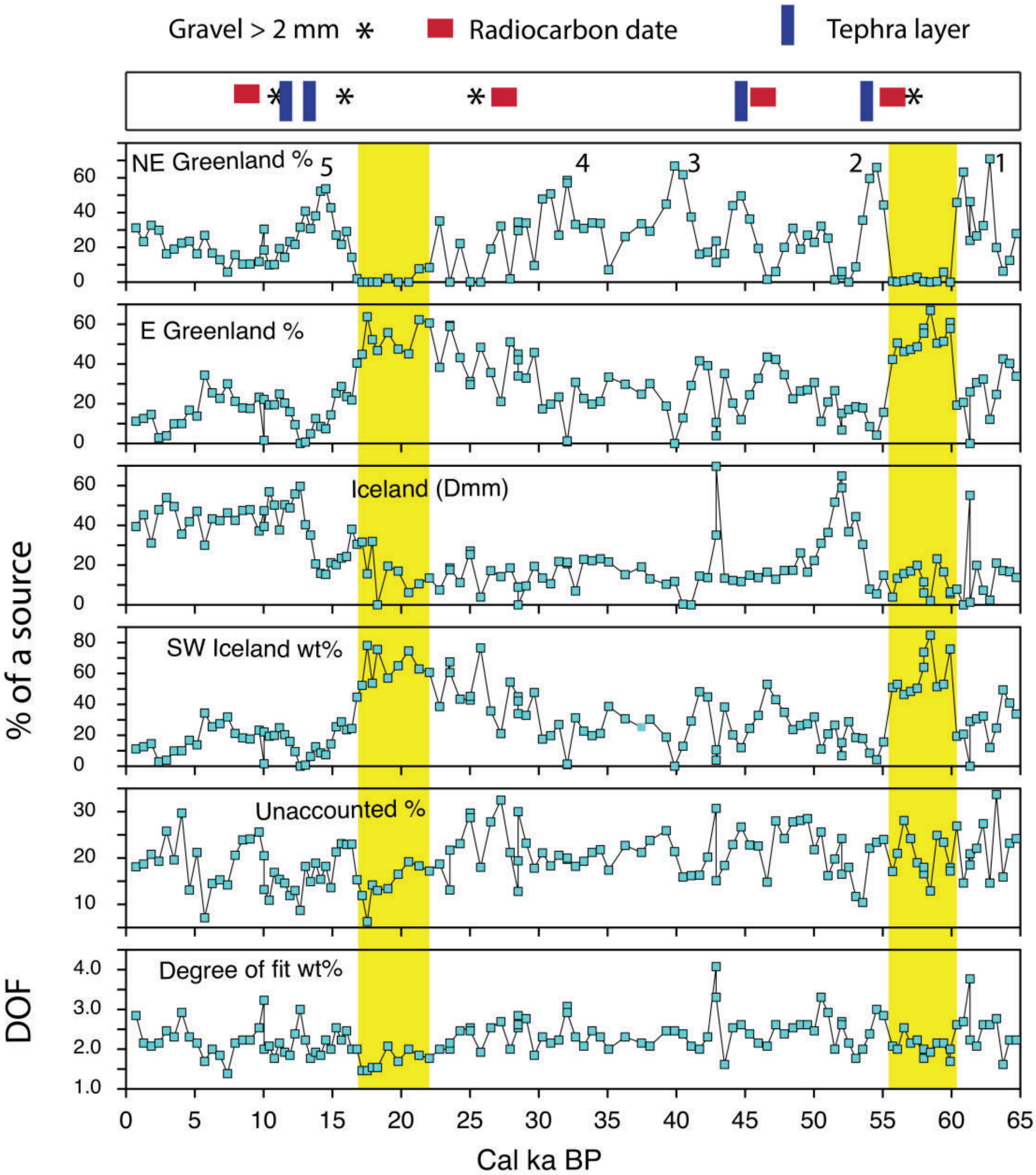

Figure 5: Plots of the sediment source percentages and the degree of fit (DOF), that is the average absolute bias in the SedUnMix calculation of (observed mineral wt% - predicted mineral weight%) for each sample. The top panel shows the location of measurable quantities of gravel, and sites of tephra layers and the radiocarbon dates on near-surface planktonic foraminifera (Table 3). Numbers on the NE Greenland panel represent the peaks in that source and the yellow bars locate areas with minimal input from that area.

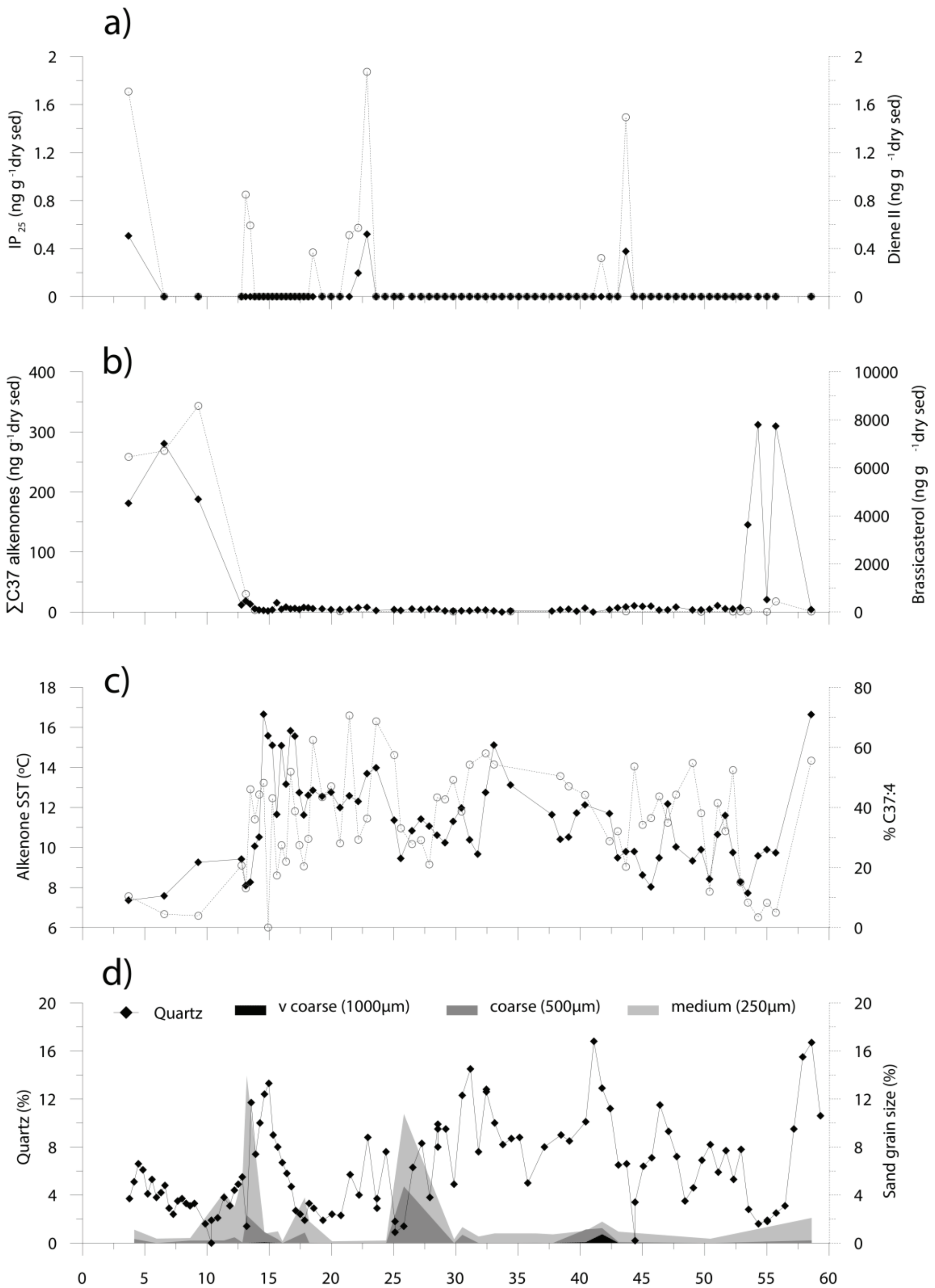

Figure 6: Biomarker data (A) IP_{25} and HBI II concentrations; (B) $\sum C_{37:3}+C_{37:2}$ alkenone and brassicasterol concentrations; C) SST° C estimates and the $\%C_{37:4}$; and D) Weight % quartz and different coarse sediment fractions.

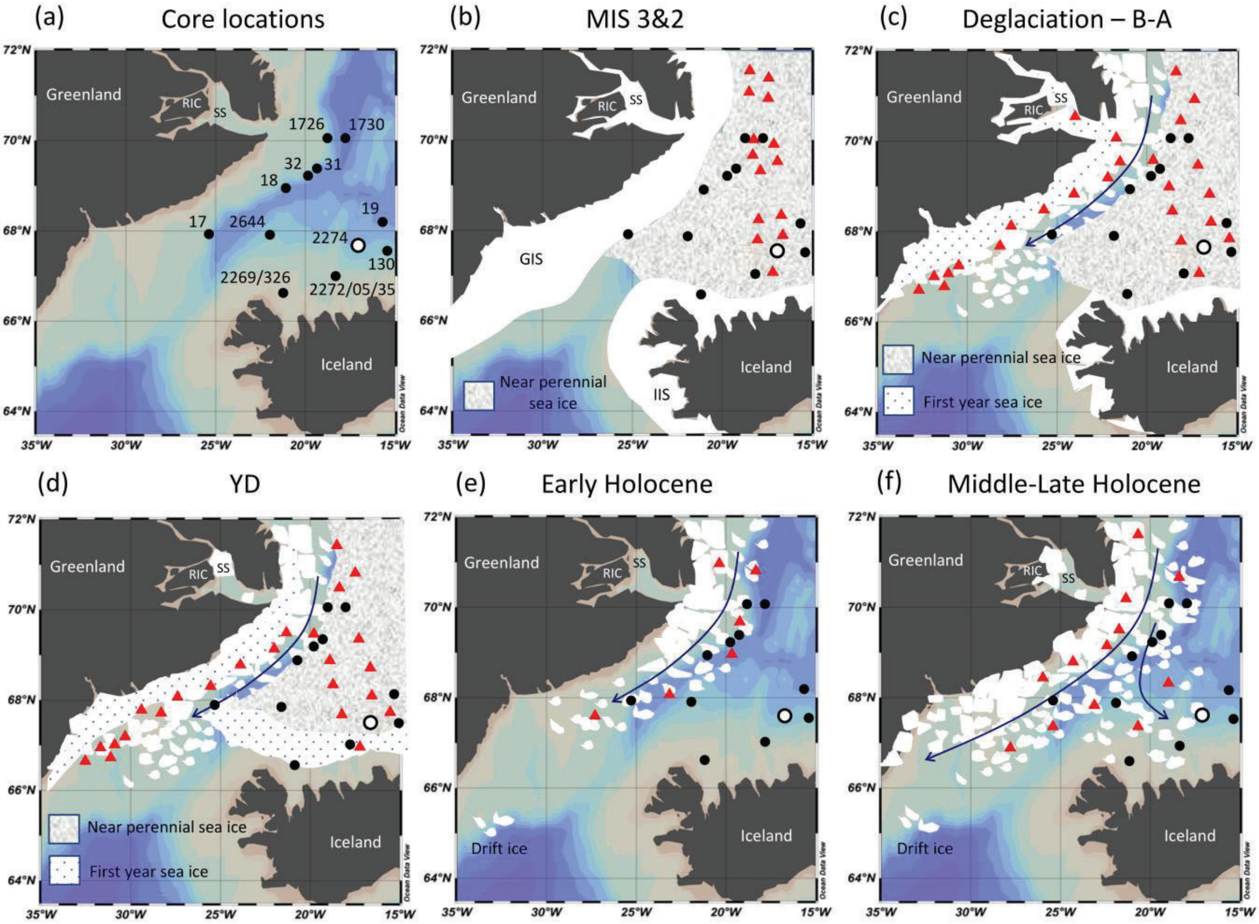

Figure 7: Schematic presentation of changes in sea ice and iceberg distribution. The first panel (upper left) shows core locations (see Table 1 and Fig. 1A and B) and the adjoining panel the inferred conditions during MIS 3 and 2 with pervasive sea ice and embedded icebergs. The remaining panels show the proposed evolution in the state of sea ice and iceberg supply (red triangles) during deglaciation into the Holocene (adapted from Cabedo-Sanz et al., 2016; Xiao et al., 2017). SS =Scoresby Sound, RIC=Renland Ice Cap.

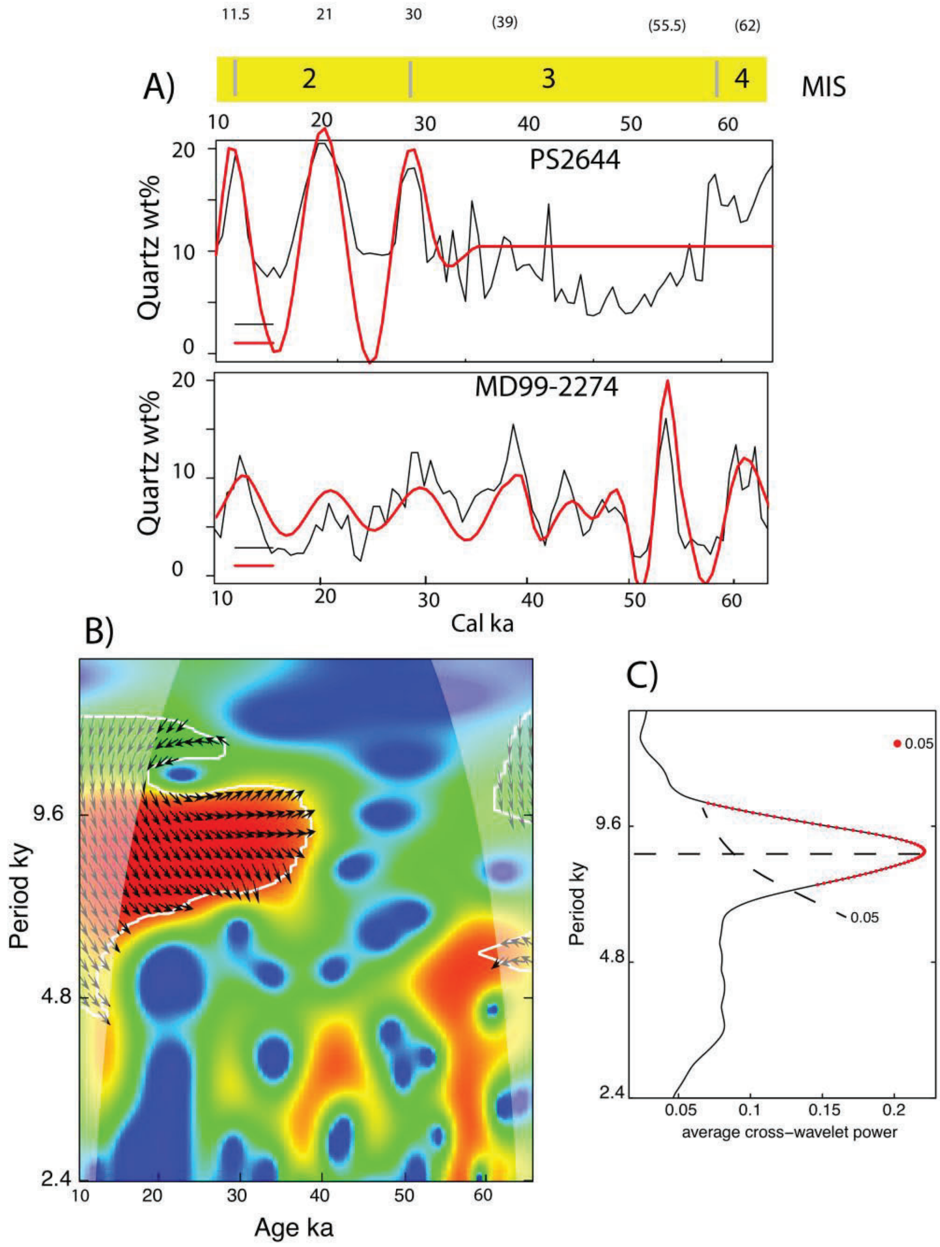

Figure 8: Analysis of the quartz wt% records from PS2644 (Vogt, 2017) and MD99-2274 at a common 0.6 ky spacing. A) Original quartz data (black line) and the wavelet reconstructions for the two records; B) Cross-wavelet power spectrum of quartz wt% for PS2644 and MD99-2274. The cone of confidence indicated by the light grey areas; 0.05% probability area demarcated by white line. Arrows pointing to the right mean that the two records are in phase, arrows pointing down mean that x leads y, arrows pointing to the left indicate the records are anti-phase and pointing up indicates that #2274 leads PS2644. C) Cross-wavelet (Fig. 8B) average power. The 0.05 significance period is red and delimited by the dashed slanting line. The horizontal dashed line indicates the peak periodicity (~8.5 ky).